AGU PUBLICATIONS

Paleoceanography

RESEARCH ARTICLE
10.1002/2015PA002825

Key Points:
- Bulk carbonate $\delta^{13}C$ and $\delta^{18}O$ data primarily record mixed layer conditions
- Coccolithophore biogeochemistry impacts bulk stable isotope records
- Data from Sites U1338 and 573 suggest enhanced upwelling between 8 Ma and 4 Ma

Supporting Information:
- Figures S1–S3
- Table S1
- Table S2

Correspondence to:
D. Reghellin,
daniele.reghellin@geo.su.se

Citation:
Reghellin, D., H. K. Coxall, G. R. Dickens, and J. Backman (2015), Carbon and oxygen isotopes of bulk carbonate in sediment deposited beneath the eastern equatorial Pacific over the last 8 million years, *Paleoceanography*, *30*, 1261–1286, doi:10.1002/2015PA002825.

Received 4 MAY 2015
Accepted 18 SEP 2015
Accepted article online 22 SEP 2015
Published online 21 OCT 2015
Corrected 11 NOV 2015

This article was corrected on 11 NOV 2015. See the end of the full text for details.

Carbon and oxygen isotopes of bulk carbonate in sediment deposited beneath the eastern equatorial Pacific over the last 8 million years

Daniele Reghellin[1], Helen K. Coxall[1], Gerald R. Dickens[1,2], and Jan Backman[1]

[1]Department of Geological Sciences, Stockholm University, Stockholm, Sweden, [2]Department of Earth Sciences, William Marsh Rice University, Houston, Texas, USA

Abstract To improve the understanding and utility of bulk carbonate stable carbon and oxygen isotope measurements, we examine sediment from cores in the eastern equatorial Pacific that span the last 8 Ma. We measured $\delta^{13}C$ and $\delta^{18}O$ in 791 samples from Integrated Ocean Drilling Program Site U1338 and Deep Sea Drilling Project Site 573, both located close to the Pacific equator. In 100 samples, we measured $\delta^{13}C$ and $\delta^{18}O$ on isolated <63 μm and <38 μm fractions, which concentrates calcareous nannofossil carbonate and progressively excludes foraminiferal carbonate. Bulk carbonate $\delta^{13}C$ and $\delta^{18}O$ records are similar to published records from other sites drilled near the equator and seem to reflect mixed layer conditions, albeit with some important caveats involving the precipitation of calcite by coccolithophores. The comparatively lower $\delta^{13}C$ and $\delta^{18}O$ of the <63 μm and <38 μm fractions in sediments younger than 4.4 Ma is attributed to an increase in deep-dwelling planktic foraminifera material in bulk carbonate, shifting the bulk isotopic signals toward higher values. Bulk carbonate $\delta^{13}C$ is similar over 2500 km along the Pacific equator, suggesting covarying concentrations and $\delta^{13}C$ of dissolved inorganic carbon within surface waters since 8 Ma. Greater bulk sediment $\delta^{13}C$ and $\delta^{18}O$, higher sedimentation rates, and low content of coarse material suggest intensified wind-driven upwelling and enhanced primary productivity along the Pacific equator between 8.0 and 4.4 Ma, although a full understanding of bulk carbonate records will require extensive future work.

1. Introduction

Temporal changes in the carbon and oxygen stable isotope composition of marine calcium carbonate lie at the heart of many paleoceanographic reconstructions [*Emiliani*, 1955; *Shackleton*, 1967; *Raymo et al*., 1989; *Zachos et al*., 2001]. For the late Cenozoic, and in unlithified sediment from regions that have remained above the lysocline, such $\delta^{13}C$ and $\delta^{18}O$ records typically are generated through measurements of planktic or benthic foraminifera tests. By contrast, the stable isotope composition of bulk carbonate is commonly used for older sediments and sedimentary rocks [*Scholle and Arthur*, 1980; *Shackleton*, 1986; *Weissert and Erba*, 2004; *Lourens et al*., 2005; *Tripati et al*., 2005; *Jarvis et al*., 2006; *Zachos et al*., 2010; *Slotnick et al*., 2012; *Voigt et al*., 2012]. The reasons for this are threefold (above references and [*Frank et al*., 1999]): (1) samples can be prepared much faster than isolated foraminifera samples, which necessitate sediment sieving and manual picking of individual specimens, (2) foraminifera tests are difficult to extract from lithified sediments, a problem that becomes increasingly common with increasing burial depth and sediment age, and (3) bulk carbonate stable isotope analyses require small sample volumes, which allows high spatial and temporal resolution, even in sections with low sedimentation rates. Foraminifera also are preferentially prone to dissolution and recrystallization of calcite, which can impact their stable isotope composition [*Killingley*, 1983; *Sexton et al*., 2006; *Pearson and Burgess*, 2008].

While bulk carbonate isotope data have been used successfully for stratigraphic correlation (above references), the ensuing paleoceanographic interpretations come with uncertainty. In large part, this is because bulk carbonate represents a mixture of multiple carbonate components that (i) can carry different stable isotope signals reflecting the ecological, metabolic, and calcification conditions of biological producers or the temperature and composition of pore waters, and (ii) may vary in relative abundance over time as a function of changes in ocean temperature, vertical mixing, and carbonate preservation.

For sediment deposited in open ocean environments over the last 100 million years, calcareous nannofossils often dominate bulk marine carbonate. This is especially true for sites deposited below the lysocline, as calcareous nannofossils are generally less susceptible to carbonate dissolution than foraminifera, especially

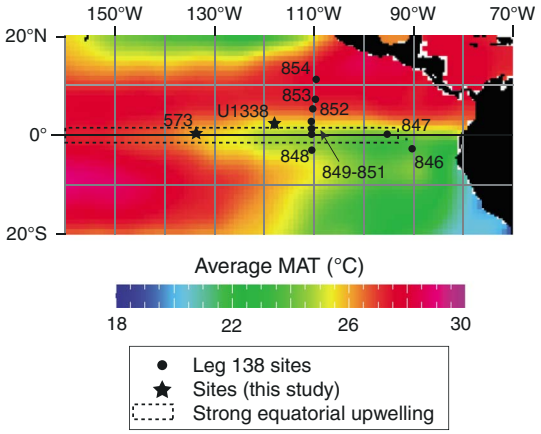

Figure 1. Map showing mean annual temperature (MAT) of EEP surface waters and Ocean Drilling Program (ODP)/Integrated Ocean Drilling Program (IODP) drill site locations. Dashed box represents the area of strong wind-driven equatorial upwelling, located west of the Galapagos Islands and about ±2° latitude of the equator.

planktic taxa [*McIntyre and McIntyre*, 1971; *Berger*, 1973a; *Anderson and Steinmetz*, 1981; *Shackleton and Hall*, 1984; *Perch-Nielsen*, 1985; *Young et al.*, 2005; *Blaj et al.*, 2009]. The study of stable isotopes in calcareous nannofossils began when *Anderson and Cole* [1975] demonstrated that the $\delta^{18}O$ of planktic foraminifera and the $\delta^{18}O$ of $<44\,\mu m$ fraction of sediment covaried systematically in Pleistocene sediments and *Margolis et al.* [1975] showed that the $\delta^{13}C$ and $\delta^{18}O$ of planktic foraminifera, benthic foraminifera, and the $<44\,\mu m$ fraction of sediment paralleled each other from the middle Eocene through the Pleistocene at three Deep Sea Drilling Project (DSDP) Sites. In both cases, the $<44\,\mu m$ fraction was taken to represent nannofossil carbonate, and offsets in the absolute $\delta^{13}C$ and $\delta^{18}O$ values of the various sedimentary phases were noted. These initial results were followed by stable isotope studies (albeit often only $\delta^{18}O$) of cultured calcareous nannoplankton [*Dudley and Goodney*, 1979; *Dudley et al.*, 1980, 1986] and bulk sediment and sieved fractions from core tops [*Goodney et al.*, 1980; *Dudley and Nelson*, 1988] and Pleistocene cores [*Anderson and Steinmetz*, 1981, 1983; *Steinmetz and Anderson*, 1984; *Paull and Thierstein*, 1987, 1990]. Importantly, these studies concluded that (i) $\delta^{13}C$ and $\delta^{18}O$ of calcareous nannoplankton relate to surface water properties, including temperature, but (ii) offsets in $\delta^{13}C$ and $\delta^{18}O$, typically 1–3‰, occurred relative to carbonate precipitated at equilibrium. These offsets are commonly referred to as "vital effects."

From a paleoceanographic perspective, the calcareous nannoplankton vital effects pose a problem to interpretations of $\delta^{13}C$ and $\delta^{18}O$ records constructed from bulk sediment and various fine-grained sediment fractions. On the other hand, the above studies clearly suggest that calcareous nannofossils carry signals of mixed layer conditions, and several papers have employed bulk carbonate stable isotopes from unlithified late Neogene sediment sequences to make seemingly plausible reconstructions of past changes in oceanography [*Ennyu et al.*, 2002; *Grant and Dickens*, 2002; *Liu et al.*, 2002]. More recently, a series of studies, focused on either culturing of calcareous nannoplankton or extracting calcareous nannofossils across intervals of past oceanographic change, have endeavored to understand the causes and consequences of the stable isotope vital effects [*Ziveri et al.*, 2003; *Stoll*, 2005; *Rickaby et al.*, 2010; *Bolton et al.*, 2012; *Bolton and Stoll*, 2013; *Candelier et al.*, 2013; *Hermoso et al.*, 2014; *Hermoso*, 2015]. It seems an opportune time to more fully appreciate bulk carbonate stable isotope records.

The eastern equatorial Pacific (EEP) represents a broad area between about 15°N and 15°S latitude and between about 150°W longitude and the coasts of Central and South America (Figure 1). In an inspirational study, *Shackleton and Hall* [1995] emphasized the potential of bulk carbonate stable isotope work in this region, where foraminifera fossils are scarce. Here we attempt to improve the utility of bulk carbonate stable isotope measurements in paleoceanographic studies by untangling the contribution of carbonate constituents in deep sea cores from the EEP that span the last 8 Ma and by trying to interpret the signals within the framework of current knowledge. Our results show that different particle size classes within bulk sediment of the EEP give similar $\delta^{13}C$ and $\delta^{18}O$ records and that these stable isotope records correlate between widely separated sites in the time domain. The combination supports longstanding ideas that bulk carbonate stable isotope records, at least in unlithified sediment, relate to conditions in the mixed layer, although the details remain perplexing.

2. Study Location and Previous Work

2.1. Paleoceanography in the EEP

The EEP has long interested the paleoceanographic community [*Arrhenius*, 1952; *Ravelo*, 2010; *Pälike et al.*, 2012; *Zhang et al.*, 2014]. This is partly because the region represents a highly sensitive and dynamic part of Earth's

ocean-climate system, characterized by high-wind-driven equatorial upwelling and substantial biological productivity [*Dunn*, 1982; *Chavez and Barber*, 1987; *Fiedler et al*., 1991; *Pennington et al*., 2006; *Lyle et al*., 2008]. It is also partly because major changes in sediment composition can be dated and correlated over a very broad region [*Farrell et al*., 1995a; *Bloomer and Mayer*, 1997].

One challenge facing studies of long-term ocean-climate variability in the EEP concerns modern oceanographic variability. Steep zonal and meridional gradients in certain surface properties, such as sea surface temperature (SST) and biological productivity, characterize the region (Figure 1). These gradients result from a range of processes but particularly the combination of wind-driven currents and upwelling of cold, nutrient-rich water [*Kessler*, 2006; *Pennington et al*., 2006]. Surface property gradients also vary significantly on interannual and intraannual time scales [*Barber and Chavez*, 1986; *Trenberth and Caron*, 2000]. Environmental heterogeneity in space and time is especially extreme west of Galapagos (>90.5W longitude), where wind-driven equatorial upwelling is strongest (Figure 1). As a consequence, paleoceanographic interpretations for the region should be based on records from multiple locations with different latitude and longitude.

A second problem concerns the depths of the seafloor and the lysocline within the EEP. The term lysocline has a range of definitions [*Boudreau et al*., 2010] but might be defined best as the water depth where an abrupt change in the rate of calcite dissolution is apparent in seafloor sediment [*Farrell and Prell*, 1989]. The lysocline lies at about 3500 to 4000 m water depth across the present EEP [*Berger*, 1973a; *Archer*, 1991] but was generally shallower for most of the Neogene [*Farrell and Prell*, 1989; *Farrell et al*., 1995a; *Lyle and Wilson*, 2006]. Given that most of the EEP seafloor lies below 4000 m, this means that carbonate tests, particularly those of foraminifera, may be impacted by dissolution.

Cores collected from the EEP show major changes in their bulk sediment composition over short intervals of depth and time [*Herbert and Mayer*, 1991; *Farrell et al*., 1995a; *Pisias et al*., 1995; *Bloomer and Mayer*, 1997; *Lyle and Wilson*, 2006]. In general, the sediments consist of variable proportions of biogenic carbonate, biogenic silica, and minor amounts of terrigenous minerals, mostly fine-grained clay [*Mayer et al*., 1985; *Pälike et al*., 2010; *Reghellin et al*., 2013]. The changes in sediment composition likely reflect variations in oceanography and preservation, although it is not easy to constrain the dominant factors [*Lyle et al*., 2010].

2.2. Published Bulk Sediment Stable Isotope Records From the EEP

Shackleton and Hall [1995] measured the $\delta^{13}C$ and $\delta^{18}O$ of bulk sediment collected from sites of Ocean Drilling Program (ODP) Leg 138 [*Pisias et al*., 1995]. The sites were drilled and cored along two north-south transects (Figure 1): a western transect (Sites 848–854) crossing the equator at about 110°W and an eastern transect (Sites 844–847) placed at about 95°W [*Mayer et al*., 1992]. *Shackleton and Hall*'s [1995] samples consisted of homogenized "scrapings" derived by smoothing (scraping) the surfaces of 150 cm split core sections.

The bulk carbonate stable isotope records show long-term secular changes over the last 3 to 15 Ma, as well as short-term Milankovitch-scale variations at sites with higher sedimentation rate (Figure 2). Across the sites, the $\delta^{13}C$ records give very similar patterns in terms of timing and amplitude of variability. This includes several large-amplitude $\delta^{13}C$ perturbations (>1‰) in the late Miocene and late Pleistocene (Figure 2). The intersite coherency in $\delta^{13}C$ seems useful for high-resolution stratigraphic correlation [*Shackleton and Hall*, 1995] and suggests region-wide forcing by processes that affect carbon cycling or the record thereof, an important recognition for studies of more ancient sequences.

Although the bulk carbonate $\delta^{18}O$ records show some intersite coherency, significant differences exist between sites located away from the modern equator (Sites 852–854) and those located on or near the modern equator (Sites 846–851). The most striking feature is an approximately 1.0‰ separation in $\delta^{18}O$ between off- and on-equator records between approximately 8 Ma and 4 Ma (Figure 2). The separation in $\delta^{18}O$ records becomes more apparent upon correction of site location with past changes in plate motion and latitude and seemingly coincides with a major increase in the accumulation of biogenic sediment components along the equator [*van Andel et al*., 1975; *Farrell et al*., 1995a]. Thus, *Shackleton and Hall* [1995] offered the following interpretation: lower SSTs occurred along the equator during the late Miocene and early Pliocene because of enhanced wind-driven upwelling that brought cool, nutrient-rich deep water to the surface. This interpretation, while perhaps consistent with some recent work [*Seki et al*., 2012; *Zhang et al*., 2014], is almost opposite to dogma presented over the last 15 years. A series of studies, mainly based on planktic foraminifera stable isotopes, planktic foraminifera Mg/Ca ratios, and alkenone ratios, allude to a late Miocene-early Pliocene EEP characterized

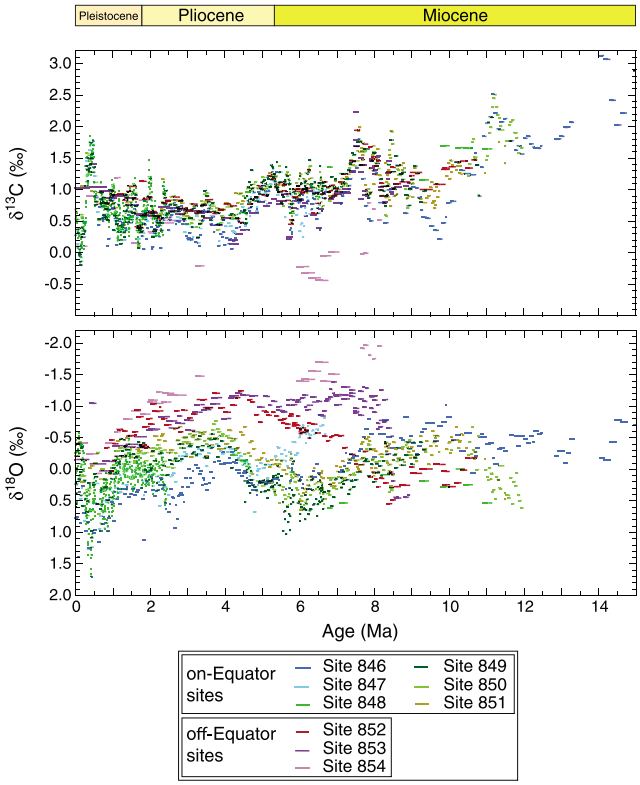

Figure 2. Bulk sediment carbon and oxygen stable isotope records [*Shackleton and Hall*, 1995] over 15 Ma from nine ODP Leg 138 sites, on the *Bergreen et al.* [1995] time scale. Data are shown as bars to symbolize that each sample represents the integrated value over a 150 cm long core section. Bar lengths reflect the duration of each sample (150 cm/LSR). Note that $\delta^{18}O$ values at Sites 849–851 are heavier than those at Sites 852–854 in the approximately 4–8 Ma interval.

by higher SSTs and weakened equatorial upwelling [*Cannariato and Ravelo*, 1997; *Ravelo et al.*, 2004; *Wara et al.*, 2005; *Brierley et al.*, 2009; *Ravelo*, 2010; *Steph et al.*, 2010; *Ford et al.*, 2015]. Although *Dickens and Backman* [2012] and *Lea* [2014] have highlighted the discrepant interpretations for late Miocene-early Pliocene oceanography across the EEP, the *Shackleton and Hall* [1995] data set largely has been ignored.

The existing stable isotope records of bulk carbonate within the EEP suggest considerable variability in past surface ocean conditions [*Shackleton and Hall*, 1995]. The causes of these changes remain unclear. This emphasizes an important issue of particular relevance to the deep-time community: what do bulk carbonate stable isotope records actually represent in terms meaningful to paleoceanography? To begin addressing this question, we have generated new bulk carbonate $\delta^{13}C$ and $\delta^{18}O$ records at two sites in the EEP. These are Integrated Ocean Drilling Program (IODP) Site U1338 and Deep Sea Drilling Project (DSDP) Site 573 and were selected because they lie near the equator but west of Leg 138 sites. Thus, they should provide information at locations where water depths are deeper and, at least at present day, where the wind-driven upwelling system is more confined (Figure 1).

We chose a sampling strategy to answer four basic questions: (1) Are the published bulk carbonate $\delta^{13}C$ and $\delta^{18}O$ records coherent across a wide distance along the Pacific equator? (2) Are the existing records from core scrapings integrating much finer centimeter- to decimeter-scale variability in stable isotopes? (3) Are the bulk carbonate records predominantly reflecting the $\delta^{13}C$ and $\delta^{18}O$ composition of the calcareous nannofossil component and therefore a surface mixed layer signal? (4) Are variations in stable isotopes, both long term and short term, coupled to changes in the proportions of nannofossil and foraminiferal carbonate?

3. Sites and Samples

3.1. IODP Site U1338

Site U1338 was drilled at 2°30.47′N latitude, 117°58.18′W longitude, and a water depth of 4200 m (Figure 1) [*Pälike et al.*, 2010]. Four holes, U1338A–U1338D, were drilled at this location, which sits on approximately 18 Ma oceanic crust. The stratigraphic record is 415 m thick, which mostly was collected using the advanced piston corer (APC), a tool designed to minimize sediment disturbance during coring [*Graber et al.*, 2002; *Pälike et al.*, 2010]. Cores from Holes A, B, and C have been aligned and placed onto a core composite below seafloor (CCSF) depth scale [*Wilkens et al.*, 2013]. We use the Site U1338 CCSF scale when discussing depths at this site but acknowledge that they are generally about 1.11 times greater than true depth (Table S1 in the supporting information).

The Site U1338 sedimentary sequence has been subdivided into four lithological units on the basis of composition, color, and physical properties [*Pälike et al.*, 2010]. The upper two units are of interest to this study

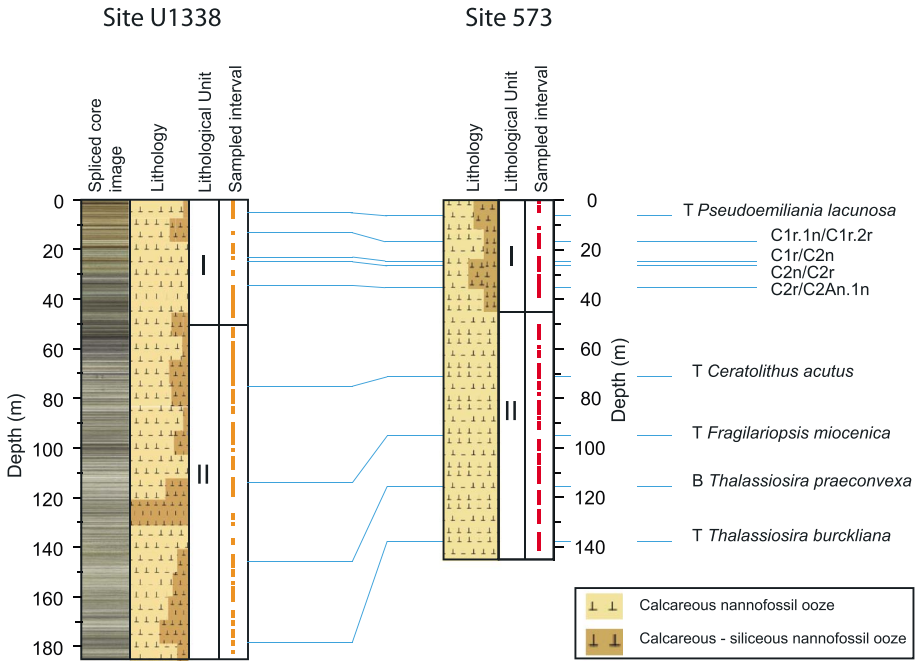

Figure 3. Lithological units of Sites U1338 [*Pälike et al.*, 2010] and 573 [*Mayer et al.*, 1985]. Site U1338 spliced core image is modified from *Wilkens et al.* [2013]; the lithological column is modified from *Lyle et al.* [2010]. Site 573 lithological column is modified from *Mayer et al.* [1985]. Correlation is based on biomagnetostratigraphy (Table 1). Sampled interval columns show locations of samples (Tables S1and S2).

(Figure 3). Unit I is 50.6 m thick and represents Pleistocene to middle Pliocene sediments. It is composed of alternating intervals of nannofossil ooze, diatom nannofossil ooze, and radiolarian nannofossil ooze. Unit II is 196.6 m thick and represents middle Pliocene to upper Miocene sediments. It is composed of alternating intervals of nannofossil ooze, diatom nannofossil ooze, nannofossil diatom ooze and radiolarian diatom ooze. Both units show striking centimeter- to decimeter-scale changes in color that relate to differences in sediment lithology, carbonate content, and physical properties (Figure 4) [*Pälike et al.*, 2010; *Reghellin et al.*, 2013; *Wilkens et al.*, 2013].

A total of 606 samples from Unit I or upper Unit II at Site U1338 were selected for this study. Each sample represents 1 to 4 plugs (a plug consists of 5 cm^3) of sediment that spans 1 to 4 cm of vertical thickness. On average, the sample spacing is 30.0 cm or 13.1 ka.

3.2. DSDP Site 573

Site 573 was drilled at 0°29.91′N latitude, 133°18.57′W longitude, and a water depth of 4301 m (Figure 1) [*Mayer et al.*, 1985]. Three holes were drilled: Hole 573* (originally Hole 573), Hole 573A, and Hole 573B. Overall, a 528 m thick sediment sequence was recovered, which lies on approximately 39 Ma oceanic crust. The upper 159.4 m were collected using the hydraulic piston corer, an early version of the APC. As such, cores retrieved from Site 573 are more disturbed than those recovered from Site U1338. Cores from the three holes have been aligned and placed onto a tentative meters composite depth (mcd) scale (Table S2). Depths on this scale are also about 1.1 times greater than true depth.

Sediments at Site 573 were divided into five lithological units on the basis of composition, with some units further divided into subunits on the basis of color [*Mayer et al.*, 1985]. The upper two units are of interest to this study (Figure 3). Unit I is 45.1 m thick and encompasses Pleistocene to upper Pliocene brown to light gray cyclic siliceous calcareous ooze. Subunit IIA comprises the uppermost 115.1 m of Unit II and represents upper Pliocene to upper Miocene sediments. It is composed of varicolored siliceous nannofossil ooze and radiolarian diatom nannofossil ooze. High-amplitude, centimeter- to decimeter-scale changes in color, carbonate content, and sediment physical properties characterize these units [*Mayer et al.*, 1985]. However, these variations are not as evident as at Site U1338, perhaps because of greater drilling disturbance.

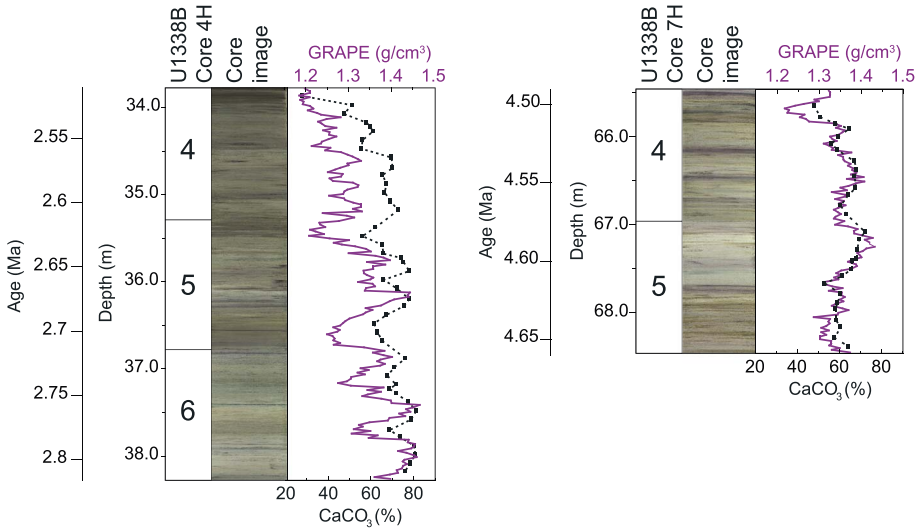

Figure 4. Images of Cores U1338B-4H (Sections 4–6) and U1338B-7H (Sections 4 and 5). These sections were selected because they have the highest resolution of carbonate content. High-resolution centimeter- to decimeter-scale variations in sediment color correspond to changes in Gamma Ray Attenuation Porosity Evaluator (GRAPE) measurements (approximating wet bulk density) and carbonate content [*Reghellin et al.*, 2013].

A total of 185 samples from Unit I or upper Subunit IIA at Site 573 were selected for study. Each sample represents two to four plugs (a plug consists of 5 cm^3) of sediment that spans 2 to 4 cm of vertical thickness. On average, the sample spacing is of 76.2 cm in depth and of 43.2 ka in time.

4. Methods

4.1. Age Models and Sedimentation Rates

Numerous biostratigraphic and magnetostratigraphic age indicators have been identified in sediment sequences at Sites U1338 and 573 (Figure 3), as well as at other sites across the EEP, including ODP Site 850. These include the top (last occurrence) or base (first occurrence) of key nannofossil and diatom species and geomagnetic reversal boundaries. Initial age models for different EEP sites have been the focus of many independent studies. For sediment deposited since 8 Ma at the three sites of specific interest to this study, the key works are Site 573 [*Baldauf*, 1985; *Barron*, 1985; *Gartner and Chow*, 1985; *Pujos*, 1985a, 1985b; *Weinreich and Theyer*, 1985; J. Backman, unpublished, 2012], Site 850 [*Mayer et al.*, 1992; *Baldauf and Iwai*, 1995; *Pisias et al.*, 1995; *Raffi and Flores*, 1995], and Site U1338 [*Pälike et al.*, 2010; *Backman et al.*, 2013; *Baldauf*, 2013].

Three basic problems confront age models at these sites: (1) geomagnetic data are lacking from certain depth intervals at one or more sites, typically when sedimentation rates are high, (2) some biohorizons are poorly resolved in terms of depth, and (3) absolute ages for various biohorizons and geomagnetic reversal boundaries have changed significantly over the last 20 years.

We have placed key Pleistocene-late Miocene biomagnetostratigraphic information at Sites U1338, 573, and 850 onto a common timescale [*Lourens et al.*, 2004]. Using this chronology (Table 1), the stable isotope records at Sites U1338, 573, and 850 can be aligned in the time domain. To estimate ages for individual samples, midpoint depths of geomagnetic reversal boundaries and/or biohorizons were used together with assumed linear sedimentation rates between successive age indicators. This will lead to small inaccuracies in the time domain because of nonlinear sedimentation rates. However, the age discrepancy should be less than 200 ka for any sample and less than 100 ka for most samples.

4.2. Sediment Processing

All 791 bulk sediment samples were freeze dried to remove pore water, and split into two aliquots. The first aliquot was used to measure carbonate content and stable isotopes of bulk sediment. Approximately 200 mg of dried sediment was taken from each sample, ground to a fine powder using an agate mortar, placed in a labeled glass tube, and stored in a desiccator.

Table 1. Age and Depths of Age Control Points From Sites U1338, 573, and 850 Used in This Study

			Site U1338	Site 573	Site 850
Event		Age (Ma)	Depth (CCSF-A)	Depth (mcd)	Depth (mcd)
	Top Section				
N	T *Pseudoemiliania lacunosa*	0.430	5.700	7.000	9.170
M	C1r.1n/C1r.2r	1.072	13.780	17.465	
	Shackleton et al. [1995a, Table 7]	1.072			21.810
	Shackleton et al. [1995a, Table 7]	1.606			31.910
M	C1r/C2n	1.778	23.520	25.120	
M	C2n/C2r	1.945	25.480	27.110	
	Shackleton et al. [1995a, Table 7]	2.118			41.970
M	C2r/C2An.1n	2.581	34.991	35.870	
M	C2An.2r/C2An.3n	3.330		45.475	
M	C2An.3n/C2Ar	3.596	49.162		74.955
N	T Reticulofenestra pseudoumbilicus	3.820		50.710	
N	T Ceratolithus acutus	5.040	75.500	71.680	115.300
D	T Fragilariopsis miocenica	6.280	114.277	95.350	175.520
D	B Thalassiosira praeconvexa	7.070	145.889	115.690	221.620
D	T Thalassiosira burckliana	7.860	178.406	137.650	263.890

The second aliquot was used for stable isotope measurements on different particle size fractions. Our rationale was that bulk carbonate comprises a mixture of different components and that these components fall into predictable size classes [*McIntyre and McIntyre*, 1971; *Paull and Thierstein*, 1987, 1990; *Broecker and Clark*, 1999, 2009; *Boeckel and Baumann*, 2004; *Frenz et al*., 2005], each potentially having different $\delta^{13}C$ and $\delta^{18}O$ values. We measured $\delta^{13}C$ and $\delta^{18}O$ on isolated $<63\ \mu m$ and $<38\ \mu m$ fine fraction portions, assuming that there will be decreasing contributions of small planktic foraminifera and foraminifera shell fragments and increasing proportions of calcareous nannofossils, as particle size fraction decreases. The 38 μm sieve was chosen because some of the late Miocene discoasters at Site U1338 exceed 20 μm [*Backman et al*., 2013].

One hundred samples for analyses were selected from the second set of aliquots (Site U1338, Table 2; Site 573, Table 3). To evaluate reproducibility, two replicate splits were separately processed and analyzed from five randomly chosen samples at Site U1338 (Table 2).

The 105 samples were rinsed twice with de-ionized water to remove constituent salts [*Reghellin et al*., 2013] and dried in an oven for approximately 36 h. Portions of each dried sample were weighed on a Sartorius LP 220 S balance with a readability of 0.001 g. Samples were then wet-sieved through 63 μm meshes using de-ionized water. The $>63\ \mu m$ coarse fraction was collected on the mesh, and the remainder was collected in clean 1000 mL beakers. The 63 μm mesh sieves with their coarse fractions were dried in an oven at 50°C for approximately 2 h. Dried particles were removed from each mesh surface using a soft brush, weighed, and stored.

The $<63\ \mu m$ fine fraction residues were allowed to settle in their beakers for approximately 48 h and then reprocessed. Most water was siphoned off. Beakers were placed in an oven at 50°C until the sediment was dry (approximately 36 h). A portion (0.5–1 g) of dry material was removed from each beaker using a clean metal spatula, ground to fine powder, and stored and labeled in glass tubes. The remainder was further sieved, repeating the steps described above but using a 38 μm mesh sieve. These sets of subsamples represent the $<63\ \mu m$ and $<38\ \mu m$ fractions of sediment.

4.3. Carbonate Analysis

Bulk sediment carbonate content was measured on the first set of aliquots, following the coulometer method applied by *Mörth and Backman* [2011]. Carbonate content was determined from the reaction of sediments with 2 mL of 2 M hydrochloric acid (HCl), which were injected into the coulometer sample tube, completely drowning the sediment sample.

4.4. Stable Isotope Analysis

Carbon and oxygen stable isotopes were measured on all 791 bulk sediment samples from Sites U1338 and 573 (Tables S1 and S2), as well as on all 105 $<38\ \mu m$ and $<63\ \mu m$ sediment fractions (Tables 2 and 3).

Table 2. Coarse Fraction Concentrations, Carbon and Oxygen Isotopes, and Carbonate Content at Site U1338

Sample										$\delta^{13}C$			$\delta^{18}O$			
Site	Hole	Core	Type	Section	Interval top (cm)	Interval bottom (cm)	Depth (CCSF-A)	Age (Ma)	Coarse fraction (>63 mm) (Wt %)	Bulk (‰)	<63 mm (‰)	<38 mm (‰)	Bulk (‰)	<63 mm (‰)	<38 mm (‰)	$CaCO_3$ (Wt %)
U1338	A	1	H	1	30	32	0.35	0.03	23.0	0.57	0.23	0.12	0.74	−0.25	−0.26	80.9
U1338	A	1	H	1	130	132	1.35	0.10	15.5	1.10	0.55	0.52	0.58	−0.29	−0.28	57.5
U1338	A	1	H	2	80	82	2.26	0.17	14.5	0.04	−0.30	−0.36	0.35	−0.40	−0.41	69.8
U1338	B	1	H	3	130	132	4.31	0.33	9.5	1.12	1.04	1.02	1.13	0.49	0.48	78.1
U1338	A	2	H	2	25	27	5.94	0.45	12.3	1.61	1.57	1.55	0.77	0.45	0.46	69.8
U1338	A	2	H	4	85	87	9.54	0.74	8.6	0.75	0.59	0.56	0.37	0.10	0.09	77.5
U1338	A	2	H	6	85	87	12.54	0.97	10.9	0.96	0.85	0.82	0.01	−0.49	−0.23	69.1
U1338	A	3	H	1	25	27	14.97	1.16	15.0	0.79	0.59	0.52	−0.36	−0.70	−0.63	57.0
U1338	A	3	H	3	85	87	18.29	1.40	12.9	0.84	0.69	0.66	−0.26	−0.58	−0.53	53.0
U1338	A	3	H	4	25	27	19.19	1.46	8.8	0.79	0.55	0.45	−0.21	−0.29	−0.35	34.7
U1338	A	3	H	5	85	87	21.29	1.62	8.0	1.07	0.87	0.74	−0.10	−0.51	−0.82	57.4
U1338	B	4	H	4	30	32	34.08	2.52	9.5	0.86	0.69	0.67	−0.28	−0.27	−0.59	47.5
U1338	B	4	H	5	30	32	35.58	2.62	9.2	0.85	0.73	0.68	−0.67	−0.79	−0.75	65.4
U1338	B	4	H	6	80	82	37.58	2.77	10.4	0.58	0.34	0.53	−0.62	−0.81	−0.67	78.8
U1338	C	5	H	2	85	87	39.92	2.93	12.5	0.51	0.38	0.61	−0.59	−0.75	−0.52	62.0
U1338	C	5	H	3	85	87	41.42	3.04	7.0	0.88	0.78	0.86	−0.34	−0.67	−0.54	37.7
U1338	C	5	H	4	85	87	42.92	3.15	10.0	0.80	0.61	0.70	−0.37	−0.74	−0.63	32.9
U1338	A	6	H	1	25	27	46.52	3.41	8.8	0.86	0.86	0.81	−0.37	−0.74	−0.94	75.9
U1338	A	6	H	3	27	29	49.54	3.62	8.1	0.70	0.62	0.61	−0.68	−1.11	−1.25	58.7
Replicate									7.8	0.70	0.54	0.59	−0.68	−1.27	−1.22	58.7
U1338	A	6	H	3	85	87	50.12	3.65	9.9	0.78	0.71	0.63	−0.64	−0.98	−1.23	50.8
Replicate									10.4	0.78	0.66	0.67	−0.64	−1.07	−1.14	50.8
U1338	A	7	H	1	85	87	57.27	4.04	15.1	0.58	0.49	0.45	−0.58	−0.67	−0.82	67.5
U1338	A	7	H	3	85	87	60.27	4.21	9.8	0.43	0.45	0.44	−0.87	−0.94	−1.00	46.9
U1338	A	7	H	4	85	87	61.77	4.29	9.0	0.78	0.59	0.66	−0.69	−0.56	−1.04	71.5
U1338	A	7	H	5	85	87	63.27	4.37	3.6	0.80	0.72	0.73	−0.82	−0.53	−0.60	67.8
U1338	A	7	H	6	85	87	64.77	4.45	4.0	0.82	0.78	0.79	−0.64	−0.41	−0.60	65.6
U1338	A	8	H	2	85	87	70.14	4.75	4.8	0.92	0.88	0.90	−0.60	−0.52	−0.44	69.0
U1338	A	8	H	3	85	87	71.64	4.83	3.3	0.95	0.87	0.89	−0.59	−0.50	−0.52	73.2
U1338	A	8	H	4	85	87	73.14	4.91	5.0	1.16	1.03	1.07	−0.42	−0.26	−0.16	74.1
U1338	A	8	H	5	85	87	74.64	4.99	4.3	0.89	0.98	0.99	−0.28	−0.46	−0.44	71.6
U1338	A	8	H	6	85	87	76.14	5.06	2.8	1.29	1.32	1.34	−0.04	−0.01	−0.17	83.2
U1338	A	9	H	2	27	29	80.43	5.20	4.7	1.14	1.08	1.09	−0.26	−0.27	−0.35	58.2
U1338	A	9	H	5	27	29	84.93	5.34	2.6	1.37	1.31	1.34	0.05	0.13	−0.13	81.5
Replicate									2.5	1.37	1.32	1.36	0.05	0.08	−0.07	81.5
U1338	A	9	H	6	85	87	87.01	5.41	4.9	1.17	1.12	1.15	−0.23	−0.42	−0.40	52.5
U1338	A	11	H	1	85	87	100.34	5.83	3.9	0.66	0.65	0.63	−0.13	−0.33	−0.35	60.7
U1338	A	11	H	3	85	87	103.34	5.93	2.8	0.19	0.14	0.13	−0.24	−0.30	−0.37	57.4
U1338	A	11	H	5	85	87	106.34	6.03	2.9	1.18	0.97	0.94	0.26	0.12	−0.04	77.8
U1338	A	12	H	1	25	27	110.66	6.16	2.1	1.32	1.10	1.14	0.51	0.34	0.24	64.9
U1338	A	12	H	1	85	87	111.28	6.18	2.6	1.03	1.10	1.10	0.61	0.39	0.41	72.6
U1338	A	12	H	2	27	29	112.22	6.21	2.2	0.87	0.89	0.94	0.82	0.58	0.49	78.2
U1338	A	12	H	2	85	87	112.81	6.23	2.8	0.96	0.99	1.05	0.69	0.44	0.53	83.3
U1338	A	12	H	6	85	87	118.74	6.39	1.9	1.03	1.00	1.02	0.51	0.39	0.51	81.7
U1338	A	14	H	3	27	29	134.60	6.79	2.1	1.01	1.00	0.96	0.59	−0.03	−0.02	57.8
Replicate									1.6	1.01	0.96	0.94	0.59	−0.12	0.05	57.8
U1338	A	14	H	4	27	29	136.23	6.83	2.1	1.31	1.35	1.32	0.76	0.40	0.46	73.8
U1338	A	14	H	5	85	87	138.34	6.88	2.3	0.80	0.83	0.86	0.45	0.00	−0.03	61.0
Replicate									2.1	0.80	0.87	0.84	0.45	−0.03	−0.13	61.0
U1338	A	15	H	1	27	29	142.10	6.98	2.3	1.16	1.12	1.07	0.19	−0.13	−0.20	46.4
U1338	A	15	H	2	85	87	144.41	7.03	1.7	1.04	1.01	1.02	0.11	0.36	0.30	70.5
U1338	A	15	H	3	85	87	145.91	7.07	1.8	1.20	1.08	1.14	0.05	0.41	0.23	69.9
U1338	A	15	H	4	85	87	147.41	7.11	1.7	1.30	1.27	1.31	0.34	0.31	0.27	86.0
U1338	A	15	H	5	85	87	148.85	7.14	1.3	0.97	0.91	0.94	0.51	0.31	0.33	86.9
U1338	A	15	H	6	85	87	150.39	7.18	1.8	0.79	0.80	0.81	0.11	0.11	0.05	77.4

Table 3. Coarse Fraction Concentrations, Carbon and Oxygen Isotopes and Carbonate Content at Site 573

Sample									Coarse fraction	$\delta^{13}C$			$\delta^{18}O$			
Site	Hole	Core	Type	Section	Interval top (cm)	Interval bottom (cm)	Depth mcd (m)	Age (Ma)	(>63 μm) (Wt %)	Bulk (‰)	<63 μm (‰)	<38 μm (‰)	Bulk (‰)	<63 μm (‰)	<38 μm (‰)	$CaCO_3$ (Wt %)
573	*	1	H	1	35	37	0.36	0.02	22.4	0.19	−0.22	−0.14	−0.49	−0.31	−0.50	85.7
573	*	2	H	3	35	37	5.36	0.33	9.0	0.95	1.03	1.06	0.54	0.55	0.53	89.4
573	*	2	H	5	35	37	8.36	0.51	10.5	0.70	0.52	0.60	0.02	−0.12	−0.21	88.3
573	*	3	H	4	39	42	16.41	1.01	9.6	0.84	0.90	0.82	−0.29	0.00	−0.02	85.5
573	*	4	H	1	36	38	21.37	1.43	15.0	0.53	0.17	0.15	−0.23	−0.29	−0.24	81.2
573	*	4	H	6	36	38	28.87	2.07	14.5	0.63	0.10	0.05	−0.30	−0.71	−0.72	71.2
573	*	5	H	2	136	138	33.37	2.40	5.7	1.11	0.95	0.94	−0.26	−0.48	−0.29	89.9
573	*	5	H	4	36	38	35.37	2.54	6.0	0.92	0.60	0.58	−0.77	−0.60	−0.47	60.3
573	*	5	H	5	26	28	36.77	2.65	11.0	0.77	0.50	0.48	−0.48	−0.23	−0.31	70.6
573	*	5	H	6	26	28	38.27	2.77	5.5	0.78	0.68	0.66	−0.84	−0.39	−0.49	80.7
573	*	5	H	6	117	119	39.18	2.84	6.3	0.94	0.67	0.63	−0.50	−0.60	−0.43	81.0
573	*	6	H	3	26	28	42.57	3.10	15.2	0.86	0.49	0.44	−0.93	−0.76	−0.84	59.4
573	*	6	H	4	26	28	44.07	3.22	13.2	1.00	0.72	0.70	−0.84	−0.58	−0.83	61.5
573	*	7	H	2	26	28	49.77	3.73	8.5	0.94	0.79	0.76	−0.85	−0.67	−0.92	81.1
573	*	7	H	3	126	128	52.27	3.91	9.3	0.53	0.40	0.34	−0.84	−0.85	−0.82	45.7
573	*	7	H	4	26	28	52.77	3.94	8.6	0.62	0.43	0.38	−0.90	−0.78	−0.87	70.3
573	*	7	H	4	126	128	53.77	4.00	7.9	0.76	0.67	0.55	−0.99	−0.77	−0.92	55.4
573	*	7	H	5	26	28	54.27	4.03	9.9	0.84	0.68	0.58	−0.89	−0.87	−0.90	56.3
573	*	7	H	6	26	28	55.77	4.11	8.9	0.78	0.65	0.63	−0.76	−0.62	−0.75	71.7
573	*	8	H	1	126	128	58.47	4.27	7.9	0.54	0.36	0.36	−0.82	−0.89	−0.84	71.9
573	*	8	H	2	26	28	58.97	4.30	7.1	0.56	0.52	0.46	−0.86	−0.71	−0.95	48.7
573	*	8	H	2	76	78	59.47	4.33	5.6	0.55	0.45	0.40	−0.74	−0.76	−0.75	59.8
573	*	8	H	3	26	28	60.47	4.39	6.9	0.90	0.76	0.84	−0.57	−0.54	−0.63	86.2
573	*	8	H	4	126	128	62.97	4.53	3.1	0.65	0.60	0.57	−0.78	−0.66	−0.81	71.5
573	*	8	H	5	26	28	63.47	4.56	5.0	0.65	0.60	0.59	−0.45	−0.52	−0.38	62.5
573	*	8	H	5	126	128	64.47	4.62	3.7	0.64	0.53	0.47	−0.34	−0.25	−0.28	71.7
573	*	9	H	2	76	78	68.97	4.88	2.5	0.96	0.87	0.78	−0.14	0.10	−0.01	85.9
573	*	9	H	2	126	128	69.47	4.91	2.9	1.09	1.09	1.15	0.03	0.25	0.27	85.9
573	*	9	H	3	126	128	70.97	5.00	3.8	1.26	1.24	1.19	0.25	0.66	0.15	85.5
573	*	10	H	4	26	28	82.97	5.63	2.0	0.78	0.80	0.80	0.28	0.35	0.14	80.6
573	*	10	H	6	26	28	85.97	5.79	2.1	1.54	1.64	1.54	0.57	0.65	0.48	91.4
573	*	10	H	6	126	128	86.97	5.84	4.1	0.61	0.63	0.49	0.03	0.16	0.09	55.6
573	*	10	H	7	26	28	87.47	5.87	3.6	0.54	0.49	0.40	−0.30	−0.17	−0.29	70.9
573	*	11	H	1	126	128	88.97	5.95	1.8	1.01	1.05	1.02	0.52	0.70	0.52	85.8
573	*	11	H	3	126	128	91.97	6.10	2.1	1.12	1.10	1.04	0.05	0.08	0.27	81.1
573	*	11	H	5	126	128	94.97	6.26	1.5	1.00	1.00	0.97	0.59	0.46	0.50	85.8
573	*	11	H	6	126	128	96.47	6.32	1.5	1.26	1.29	1.21	0.73	0.53	0.94	92.8
573	*	11	H	7	16	18	96.87	6.34	2.0	1.16	1.28	1.18	0.99	0.86	1.00	93.5
573	*	12	H	1	26	28	97.47	6.36	1.0	1.28	1.37	1.29	0.83	0.98	0.83	91.7
573	*	12	H	2	76	78	99.47	6.44	2.6	1.17	1.20	1.23	0.68	0.68	0.67	92.9
573	*	12	H	2	126	128	99.97	6.46	1.7	1.07	1.14	1.07	0.39	0.68	0.35	90.6
573	*	12	H	3	126	128	101.47	6.52	1.3	1.31	1.40	1.33	0.17	0.83	0.50	85.7
573	*	13	H	2	126	128	108.77	6.80	2.0	0.90	1.04	0.98	0.28	0.11	0.04	81.0
573	*	14	H	1	126	128	115.87	7.08	1.5	1.38	1.36	1.32	0.53	0.39	0.51	91.4
573	*	14	H	2	26	28	116.37	7.09	1.0	1.21	1.16	1.17	0.65	0.49	0.54	94.6
573	*	14	H	2	76	78	116.87	7.11	1.7	1.10	1.06	1.03	0.09	−0.04	0.22	90.8
573	*	14	H	3	126	128	118.87	7.18	1.0	1.17	1.11	1.06	0.17	0.22	0.29	90.4
573	*	14	H	7	26	28	123.87	7.36	2.2	1.20	1.09	1.03	−0.03	−0.01	0.23	81.2
573	*	15	H	2	26	28	125.87	7.44	2.6	1.29	1.16	1.10	−0.14	−0.12	−0.18	81.1
573	*	15	H	6	26	28	131.87	7.65	2.1	1.34	1.33	1.26	0.33	0.25	0.35	85.7

The analyzed bulk sediment is composed of mixtures of biogenic carbonate and biogenic silica. The phosphoric acid used to dissolve carbonate for isotopic analysis cannot break the bond between silicon and oxygen in the biosilica. It follows that both the carbon and oxygen isotope data generated represent the carbonate component.

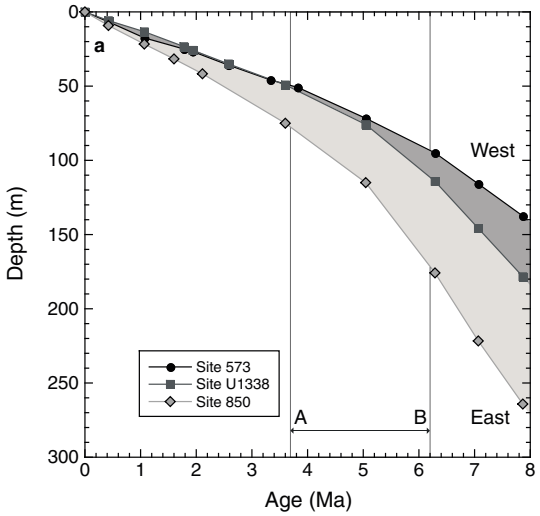

Figure 5. Age-depth model for Sites U1338, 573, and 850. LSRs are based on data listed in Table 1. The A-B segment represents the 3.596–5.04 Ma interval during which the largest decrease of LSRs occurs at Sites U1338 and 850. LSRs increase from the west to the east.

Stable isotopes were measured using a Finnigan MAT 252 IRMS coupled with a Finnigan Gasbench II device at the Department of Geological Sciences of Stockholm University. Two international standards (NBS19 and IAEA-CO-1) and two in-house standards (Carm-1 and $CaCO_3$ Merck) were analyzed with samples to evaluate accuracy and precision of isotope measurements [*Révész and Landwehr*, 2002]. The standard analytical precision based on replicate analyses of standards is ±0.06‰ for $\delta^{13}C$ and ±0.15‰ for $\delta^{18}O$. All results are given in conventional per mil (‰) notation with Vienna Pee Dee Belemnite as the reference standard.

4.5. Scanning Electron and Light Microscopy

In order to scrutinize the composition of the different size fractions and the preservation state of the biogenic carbonate components, we imaged the bulk sediment and the fine fractions of three samples from Site U1338. The four samples (U1338A-1H-1, 110–111 cm, 0.09 Ma; U1338B-1H-4, 80–82 cm, 0.40 Ma; U1338A-7H-2, 120–121 cm, 4.14 Ma; and U1338A-12H-1, 102–103 cm, 6.30 Ma) were chosen from different time slices with different coarse fraction percentages to cover a large range in $\delta^{18}O$ of bulk carbonate (Table S1).

A sticky carbon disc was placed on a 12.5 mm diameter stub. About 1–2 mg of each sample component was smeared on the surface of the carbon disc and allowed to dry overnight. Samples were gold coated for 60 s using an agar sputter coater and analyzed using a Fei Quanta Feg 650 Environmental Scanning Electron Microscope (ESEM) at the Department of Geological Sciences of Stockholm University.

For the coarse fraction (>63 μm), dried samples were imaged using a Leica M250C stereomicroscope equipped with a Leica DFC295 digital microscope camera.

5. Results

5.1. Linear Sedimentation Rates

Age/depth models from Sites U1338, 573, and 850 indicate that linear sedimentation rates (LSRs) changed significantly over the last 8 Ma (Figure 5). At Site U1338, long-term LSRs range between 41 m/Myr (7.86–7.07 Ma) and 12 m/Myr (1.95–1.78 Ma) and average 21 m/Myr (Table 1 and Figure 5). At Site 573, LSRs vary between 28 m/Myr (7.86–7.07 Ma) and 11 m/Myr (1.78–1.07 Ma) and average 16 m/Myr (Table 1). LSRs at Site 850 are generally higher, varying between 58 m/Myr (7.07–6.28 Ma) and 19 m/Myr (1.61–1.07 Ma) and averaging 32 m/Myr (Table 1). Note that, for more detailed comparisons, such LSR estimates need to be adjusted for sediment compaction as well as artificial lengthening through the use of composite depth scales. Nonetheless, the three sites exhibit coherent long-term sedimentation rate patterns. Along the equator, LSRs generally decrease to the west throughout the late Neogene, but also decrease significantly from about 6 Ma to about 4 Ma (Figure 5). Differences in the timing of LSR fluctuations at the three sites may stem from uncertainties in the depth placement of age indicators.

5.2. Grain Size

Bulk sediment grain size, represented by weight percent coarse fraction, varies significantly over depth and time at both Sites U1338 and 573 (Figures 6a and 6c). The subset of 50 samples analyzed from Site U1338 shows variations in coarse fraction (wt %) between 1% (U1338A-15H-5, 85–87 cm; 7.14 Ma) and 23% (U1338A-1H-1, 30–32 cm; 0.03 Ma) with an average of 7% (Table 2). For the 50 samples from Site 573, weight percent coarse fraction ranges between 1% (573*-14H-2, 26–28 cm; 7.09 Ma) and 22% (573*-1H-1, 35–37 cm; 0.02 Ma) with

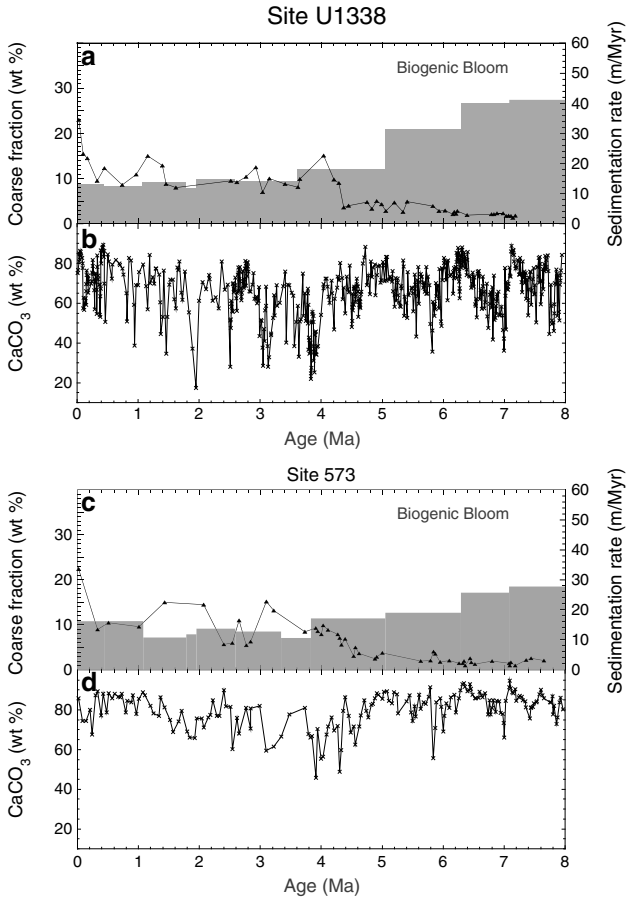

Figure 6. (a, c) Coarse fraction content (>63 μm) and LSR and (b, d) carbonate content over the past 8 Ma at Sites U1338 and 573. Biogenic Bloom shows high carbonate accumulation rates and increased biological productivity in the EEP during late Miocene and early Pliocene times.

an average of 6% (Table 3). All five replicate samples from Site U1338 render similar coarse fraction measurements, differing by only 0.3 to 0.6% for any sample (Table 2).

At both Sites 573 and U1338, the coarse fraction increases with decreasing age and depth (Figure 6). The coarse fraction is consistently lower than 5% from about 8.0 Ma until about 4.4 Ma. In younger sediment, however, most values range between 8 and 15%.

5.3. Carbonate Content

Bulk sediment carbonate content shows high variability (Figures 6b and 6d). At Site U1338, carbonate contents range between 17% (U1338C-5H-4, 85–87 cm; 3.15 Ma) and 89% (U1338A-15H-5, 85–87 cm; 7.14 Ma) with a mean of 67% (Table S1). At Site 573, carbonate content ranges between 46% (573*-7H-3, 126–128 cm; 3.91 Ma) and 95% (573*-14H-3, 26–28 cm; 7.09 Ma) with a mean of 80% (Table S2). At both sites the carbonate records display lower values between approximately 4.4 and 1.8 Ma. In this time period, mean carbonate content is 12% lower at Site U1338 and 11% lower at Site 573 compared to older and more recent times.

5.4. Carbon Isotope Composition of Bulk Sediment

Stable carbon isotope records of bulk sediment at Sites U1338 and 573 (Tables S1 and S2) exhibit similar patterns. These include long-term trends and short-term variations (Figures 7a and 8). Over the entire interval, $\delta^{13}C$ averages 0.87 ± 0.35‰ (1σ) at Site U1338 and 0.96 ± 0.35‰ (1σ) at Site 573. However, the amplitude range is slightly greater at Site U1338 than at Site 573 (Figure 7b).

The data sets can be subdivided into three segments on the basis of $\delta^{13}C$ values and age. Considering all samples from both sites, $\delta^{13}C$ is 1.43 ± 0.74‰ between 8.0 and 7.5 Ma (n = 63), 1.01 ± 0.82‰ between 7.5 and 4.5 Ma (n = 376), and 0.64 ± 0.99‰ between 4.5 and 0.5 Ma (n = 280).

Beyond the similar long-term trends, high-amplitude short-term variations occur at both sites (Tables S1 and S2). Down-core bulk sediment $\delta^{13}C$ may differ up to 1.00‰ over <1.0 m (<100 ka). For example, $\delta^{13}C$ increases by 0.99‰ between 6.89 m and 6.14 m (50 ka) at Site U1338.

5.5. Oxygen Isotope Composition of Bulk Sediment

Stable oxygen isotope records of bulk sediment at Sites U1338 and 573 (Tables S1 and S2) display similar long-term trends over the past 8 Ma (Figure 9a). Large amplitude variations are also found over short intervals (Figure 8). For all samples, the $\delta^{18}O$ averages −0.11 ± 0.40‰ (1σ) at Site U1338 and −0.06 ± 0.45‰ (1σ) at Site 573. The amplitude range is slightly lower at Site 573 than at Site U1338 (Figure 9b).

As for $\delta^{13}C$, bulk sediment $\delta^{18}O$ records can be subdivided into segments on the basis of long-term variations. Between 8.0 Ma and about 6.3 Ma, average $\delta^{18}O$ increases by 0.90‰, shifting from −0.30 ± 0.63‰ (n = 24;

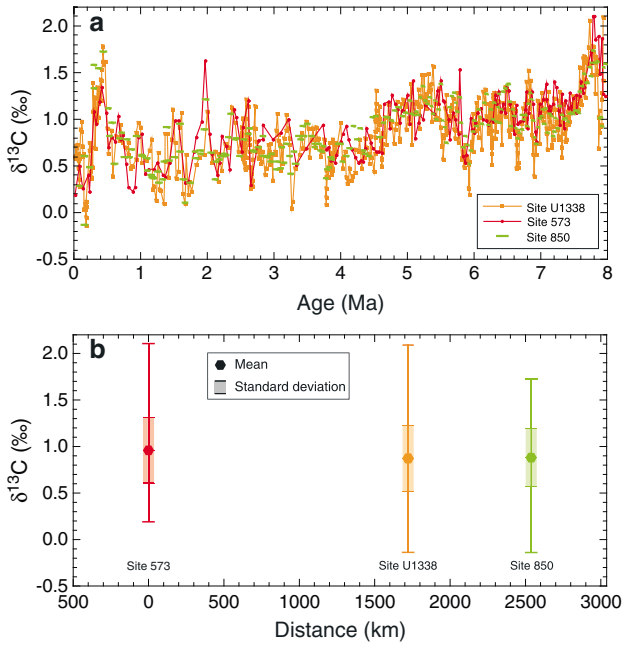

Figure 7. Comparison of $\delta^{13}C$ records for bulk sediment at near-equator sites of the EEP. Site 850 data are from *Shackleton and Hall* [1995]. (a) Time scale from *Lourens et al.* [2004]. Note similarities at the three locations over the entire 8 Ma interval and the lower amplitude variability at Site 850. (b) Statistics of bulk $\delta^{13}C$ records plotted as a function of distance between Sites 573, 850, and U1338. Mean values and standard deviations of $\delta^{13}C$ are similar at the three sites, and the amplitude range is greater at Site U1338 than at Sites 573 and 850.

8.0–7.8 Ma) to 0.60 ± 0.39‰ (n = 20; 6.4–6.3 Ma). Average $\delta^{18}O$ values thereafter decrease by 1.35‰, reaching a minimum of −0.76 ± 0.52‰ (n = 16; 3.8–3.6 Ma) centered at about 3.7 Ma. The $\delta^{18}O$ records thereafter increase by about 0.36‰, reaching a maximum −0.39 ± 0.68‰ (n = 7) at about 1.2 Ma. Beginning at 1.2 Ma, large short-term variations occur in the $\delta^{18}O$ records. For example, at Site U1338, between 5.31 m and 4.96 m, $\delta^{18}O$ becomes lower by 1.78‰ over 35 cm (30 ka). After 0.4 Ma, the $\delta^{18}O$ decreased by about 0.70‰, reaching values of −0.17 ± 0.66‰ (n = 16; 0.1–0.0 Ma). In summary, bulk sediment $\delta^{13}C$ and $\delta^{18}O$ show high variability over long and short time increments at both sites (Figures 7 and 9).

5.6. Carbon Isotopes of Size Fractions

Like the $\delta^{13}C$ of bulk sediment, the $\delta^{13}C$ of the <63 μm and <38 μm fractions (Tables 2 and 3) show distinct variability over the past 8 Ma (Figure 10). The general patterns in $\delta^{13}C$ are similar for bulk sediment and fine fractions, with some differences.

For the 50 samples sieved at Site U1338, the $\delta^{13}C$ averages 1.00 ± 0.29‰ (1σ) for bulk sediment, 0.94 ± 0.34‰ (1σ) for the <63 μm fraction, and 0.95 ± 0.34‰ (1σ) for the <38 μm fraction. The maximum amplitude in $\delta^{13}C$ is 1.64‰ for bulk sediment, 1.88‰ for the <63 μm fraction, and 1.91‰ for the <38 μm fraction. Between 8 and 4.3 Ma, the $\delta^{13}C$ signatures of all three fractions are nearly indistinguishable. After 4.3 Ma, however, the $\delta^{13}C$ records diverge slightly, with the <63 μm and <38 μm fractions having $\delta^{13}C$ values from 0.1 to 0.6‰ lower than those for bulk sediment, with the <38 μm fraction showing the lowest values (Figure 10a).

A similar pattern is seen for the 50 samples sieved at Site 573. The $\delta^{13}C$ averages 0.92 ± 0.29‰ (1σ) for bulk sediment, 0.83 ± 0.38‰ (1σ) for the <63 μm fraction, and 0.79 ± 0.37‰ (1σ) for the < 38 μm fraction. The maximum amplitudes are 1.73‰ (bulk), 1.86‰ (<63 μm), and 1.68‰ (<38 μm). The differences among the three fractions are minor prior to 4.5 Ma. After 4.5 Ma the $\delta^{13}C$ curves diverge with bulk sediment values being approximately 0.20‰ higher than those obtained from the two finer size fractions, with the <38 μm fraction typically showing the lowest values (Figure 10d).

The five samples from Site U1338 that were processed and analyzed twice provide 15 $\delta^{13}C$ measurements. Thus, each of these samples has two measurements for bulk sediment, the <63 μm fraction, and <38 μm fraction (Table 2). Five of the replicated analyses have a difference of 0.00‰, while the remaining 10 differ between 0.00 and 0.07‰. These data indicate a high precision in stable isotope measurements and provide confidence in the bulk-sieving method to deliver a reproducible geochemical signal.

5.7. Oxygen Isotopes of Size Fractions

The $\delta^{18}O$ data of the <63 μm and <38 μm size fractions (Tables 2 and 3) give rise to similar long-term trends and variability. Although some differences occur over time between the $\delta^{18}O$ of bulk sediment and the $\delta^{18}O$ of different size fractions, such relationships are not as clear as for $\delta^{13}C$ (Figure 10).

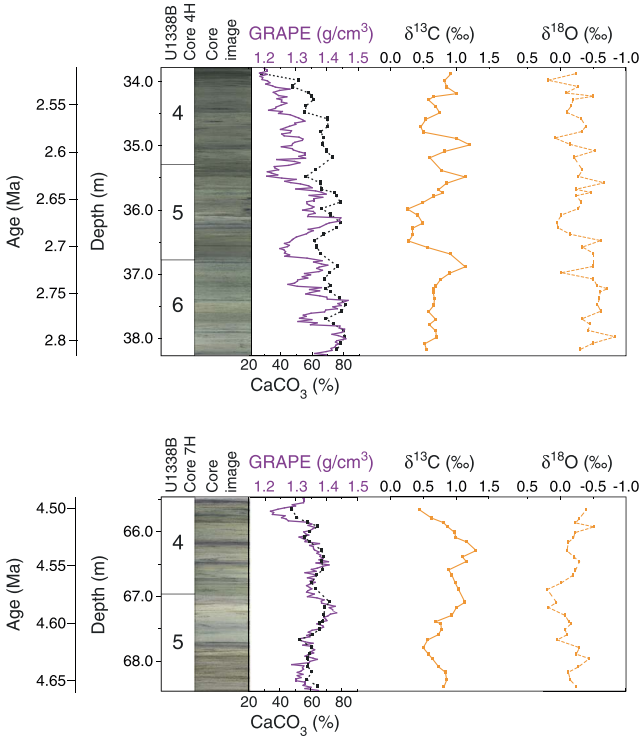

Figure 8. Images of Cores U1338B-4H (Sections 4–6) and U1338B-7H (Sections 4 and 5). These sections were selected because they have the highest resolution of carbonate content and stable isotopes. High-resolution centimeter- to decimeter-scale variations in sediment color correspond to changes in Gamma Ray Attenuation Porosity Evaluator (GRAPE) measurements (approximating wet bulk density), carbonate content [*Reghellin et al.*, 2013], and bulk sediment stable carbon and oxygen isotopes (Tables S1 and S2).

At Site U1338, the size fractions are depleted in ^{18}O compared to bulk carbonate. Considering the 50 sieved samples, $\delta^{18}O$ averages 0.00 ± 0.52‰ (1σ) for bulk sediment, −0.11 ± 0.46‰ (1σ) for the <63 μm size fraction, and −0.17 ± 0.48‰ (1σ) for <38 μm size fraction. The maximum amplitude is 2.00‰ for bulk sediment, 1.69‰ for the <63 μm size fraction, and 1.79‰ for the <38 μm size fraction. Importantly, the major ~1.5‰ decrease observed in bulk sediment $\delta^{18}O$, between about 6 and 4 Ma, is recorded in both size fractions (Figure 10b). After 4.2 Ma, there is also a change across the different size fractions, with the $\delta^{18}O$ of bulk sediment becoming 0.1–1.0‰ greater than that of the <63 and <38 μm size fractions.

Somewhat similar observations are found at Site 573. Across the 50 sieved samples, $\delta^{18}O$ averages −0.15 ± 0.57‰ (1σ) for bulk sediment, −0.09 ± 0.55‰ (1σ) for <63 μm size fraction, and −0.12 ± 0.57‰ (1σ) for <38 μm size fraction. The range in $\delta^{18}O$ composition is 1.98‰ for bulk sediment, 1.87‰ for the <63 μm size fraction, and 1.94‰ for the <38 μm size fraction. As at Site U1338, the prominent 1.5‰ decrease in $\delta^{18}O$ occurs in all size fractions (Figure 10e). However, the $\delta^{18}O$ of bulk sediment does not consistently become greater than the $\delta^{18}O$ of the size fractions after 4.2 Ma at Site 573.

As noted above for $\delta^{13}C$ analyses, each of the five samples processed and analyzed in replicate give similar $\delta^{18}O$ analyses (Table 2). For the 15 total replicate analyses of $\delta^{18}O$, five differ by 0.00‰, eight differ between 0.00 and 0.10‰, and two differ between 0.10 and 0.15‰.

5.8. Microscopic Characterization of EEP Sediments

ESEM analysis provides visual documentation of bulk sediment composition and preservation quality (Figures 11 and S1–S3). Images show variable amounts of calcareous nannofossils, siliceous tests, and foraminifera, although the latter is never a major component (Table 4). There are also major differences in the abundance and size of biogenic particles across samples, although this is difficult to demonstrate with single fields of view (Figures 11 and S1–S3). The <63 μm and <38 μm fractions of each sample contain increasing proportions of smaller particles, which are dominated by calcareous nannofossils.

Calcareous nannofossils are generally well preserved in all samples, as indicated by the presence of well-defined structural characteristics such as coccolith rims, bridges, ridges, and sutures (Figure 11d). Signs of nannofossil dissolution, such as broken coccoliths, etched coccoliths, and fragmentation, appear in some samples (Figure 11d). Importantly, though, there is little evidence of recrystallization and overgrowth of nannofossil calcite, as generally observed for the middle late Miocene through Pleistocene interval [*Pälike et al.*, 2010; *Backman et al.*, 2013]. By contrast, foraminifera typically occur as fragments of larger adult shells with occasional juvenile forms (Figures 11a and 11d). Moreover, foraminiferal carbonate shows signs of extensive

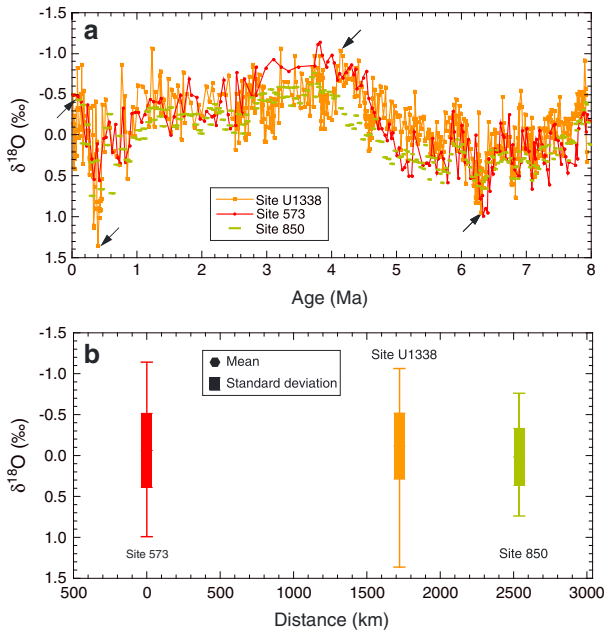

Figure 9. Comparison of $\delta^{18}O$ records for bulk sediment at near-equator sites of the EEP. Site 850 data are from *Shackleton and Hall* [1995]. (a) Time scale from *Lourens et al.* [2004]. Note similarities at the three locations over the entire 8 Ma interval and the lower amplitude variability at Site 850. Black arrows indicate samples imaged for composition and carbonate preservation of bulk sediment and isolated size fractions (Figures 11, 12, and S1–S3). (b) Statistics of bulk $\delta^{13}C$ records plotted as a function of distance between Sites 573, 850, and U1338. Mean values and standard deviations of $\delta^{18}O$ are similar at the three sites, and the isotopic amplitude range is greater at Site U1338 than at Sites 573 and 850.

dissolution and recrystallization in all samples examined (Figure 11d). The differences in area/volume ratios probably explain differences in the dissolution susceptibility and recrystallization mode of the two groups.

Light microscopy images illustrate that the >63 μm fraction in selected samples from Site U1338 consists of foraminifera tests, foraminifera fragments, radiolarian tests, and diatom frustules (Figure 12). The abundance of foraminifera tests and fragments generally increases with decreasing sediment age and increasing bulk sediment carbonate content. Partially dissolved and fragmented foraminifera tests are common to abundant in all samples. The planktic assemblage in the shallowest samples (i.e., Section U1338A-1H-1), where planktic foraminifera particles represent >50% of the coarse fraction [*Pälike et al.*, 2010], are dominated by *Globorotalia tumida*, *Globorotalia menardii*, and *Neogloboquadrina dutertrei* (Figure 12), all thermocline- or subthermocline-dwelling taxa, with only occasional examples of taxa typical of warm shallower surface mixed layer levels, such as *Globigerinoides* and *Globigerinella*. The assemblage is not representative of the settling assemblage; rather, it comprises the group of most dissolution-resistant taxa, which follows a predictable and well documented pattern that is utilized in "foraminiferal dissolution indices" [*Berger*, 1979; *Conan et al.*, 2002]. The fragmented foraminiferal elements mirror the assemblage of whole specimens, with elongate segments of broken *Globorotalia* keels, being very abundant in many samples (Figure 12).

6. Discussion

6.1. Stable Carbon and Oxygen Isotopes of Bulk Sediment Across the EEP

Carbonate content across our samples ranges from 17 to 95% by mass (Tables S1 and S2), similar to that determined at other sites along the equator in the EEP [*Farrell and Prell*, 1989; *Archer*, 1991; *Snoeckx and Rea*, 1995; *Lyle*, 2003]. This large variation in $CaCO_3$ content strongly relates to an antithetical variation in biogenic silica content [*Berger*, 1973b; *Lyle et al.*, 2010; *Reghellin et al.*, 2013]. Given that the stable isotope composition of bulk sediment determined through the reaction with phosphoric acid should closely approximate that of bulk carbonate, we discuss our stable isotope records as representing bulk carbonate.

Shackleton and Hall [1995] showed similar patterns in bulk carbonate $\delta^{13}C$ records for sediment deposited since 8 Ma at nine ODP Leg 138 sites within the EEP (Figure 2). Our new bulk carbonate $\delta^{13}C$ records from Sites U1338 and 573 are consistent with their observation but extend it ~2500 km to the west (Figure 1). This is evident by comparing the new bulk carbonate $\delta^{13}C$ records to the bulk carbonate $\delta^{13}C$ record at Site 850 on a common time scale (Figure 7). Site 850 was chosen because its latitude (1°18′N) lies about halfway between those of Sites U1338 and 573.

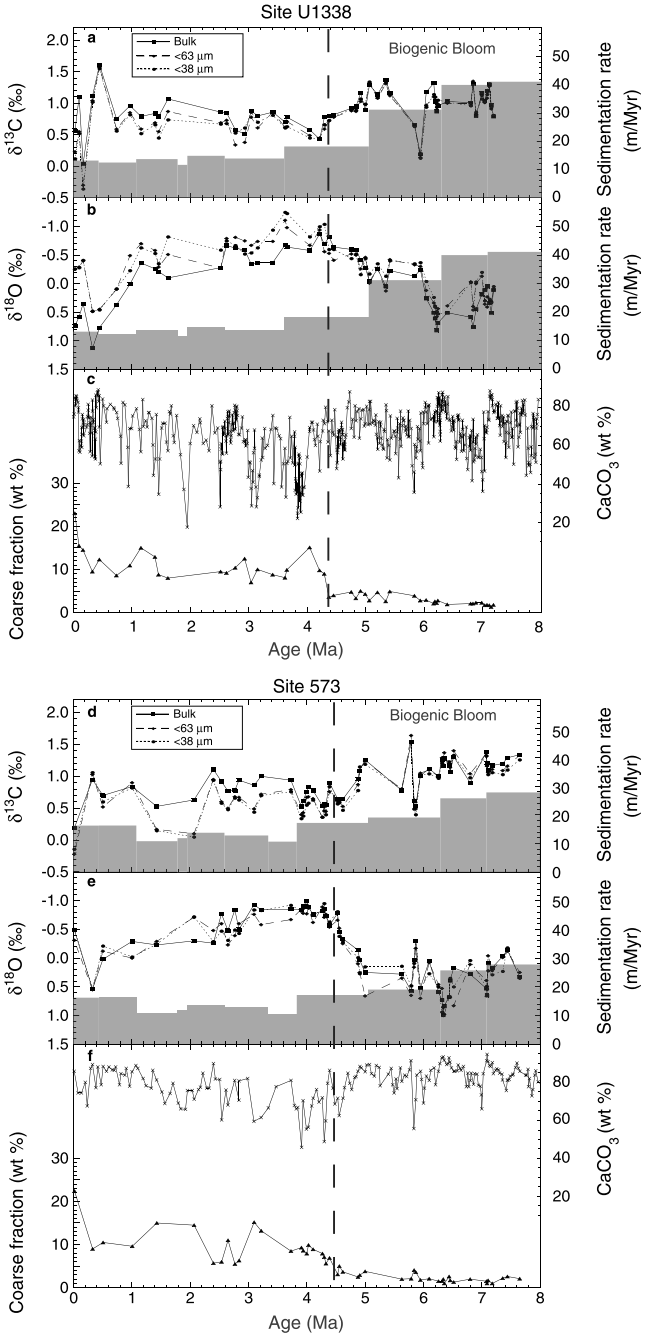

Figure 10. (a, d) Carbon and (b, e) oxygen stable isotope data of the bulk, <63 μm, and <38 μm fractions, LSRs, and (c, f) coarse fraction (>63 μm) and carbonate content over the past 8 Ma at Sites U1338 and 573. Biogenic bloom shows high carbonate accumulation rates and elevated biological productivity in the EEP during late Miocene and early Pliocene times. Note similarity in isotopic values in the 8–4.4 Ma interval, where LSRs and carbonate contents are high and coarse fraction content is <5%, and lack of correspondence between carbonate contents and stable isotopes.

Small temporal (<0.1 Ma) discrepancies exist in the bulk carbonate $\delta^{13}C$ records at the three sites (Figure 7). Examples are the peak in $\delta^{13}C$ at 7.7–7.8 Ma, the low in $\delta^{13}C$ at 4.5–4.6 Ma, and the peak in $\delta^{13}C$ at 1.9–2.0 Ma (Figure 7). Such offsets may be real and represent genuine leads and lags in carbon system fluctuations across a large area. However, the offsets could also reflect limitations of the adopted age models at the different sites.

A more obvious difference in the bulk carbonate $\delta^{13}C$ records concerns amplitude. The published Site 850 record shows lower variability in $\delta^{13}C$ with respect to time and depth than the records at Sites U1338 and 573 (Figure 7). As evident in the data from Site U1338, $\delta^{13}C$ variations on the order of 1.50‰ can occur within 150 cm intervals (Table S1 and Figure 8). The sampling method is probably at play here, as each sample at Site 850 typically represents the homogenization of short-term (10–100 ka) variations over a 150 cm long core section.

In contrast to the correlative variations in bulk carbonate $\delta^{13}C$ across the EEP, *Shackleton and Hall* [1995] showed pronounced differences in bulk carbonate $\delta^{18}O$ records at Leg 138 sites, particularly during the time interval between 8 and 4 Ma (Figure 2). Notably, bulk carbonate became enriched in ^{18}O during the latest Miocene and earliest Pliocene at sites near the equator. The new $\delta^{18}O$ records from Sites U1338 and 573, which lie close to the equator (Figure 1), parallel each other with comparable trends and average values over the last 8 Ma (Figure 9). As for $\delta^{13}C$, the $\delta^{18}O$ records from Sites U1338 and 573 show greater short-term variability than found at Site 850 (Figure 9b), presumably because signals at the latter site have been dampened through sampling style. Importantly, the new stable isotope records also exhibit distinct lows in $\delta^{18}O$ that occur between 8 and 4 Ma (Figure 9). Clearly, low $\delta^{18}O$ values characterize bulk carbonate deposited along the Pacific equator between 8 and 4 Ma.

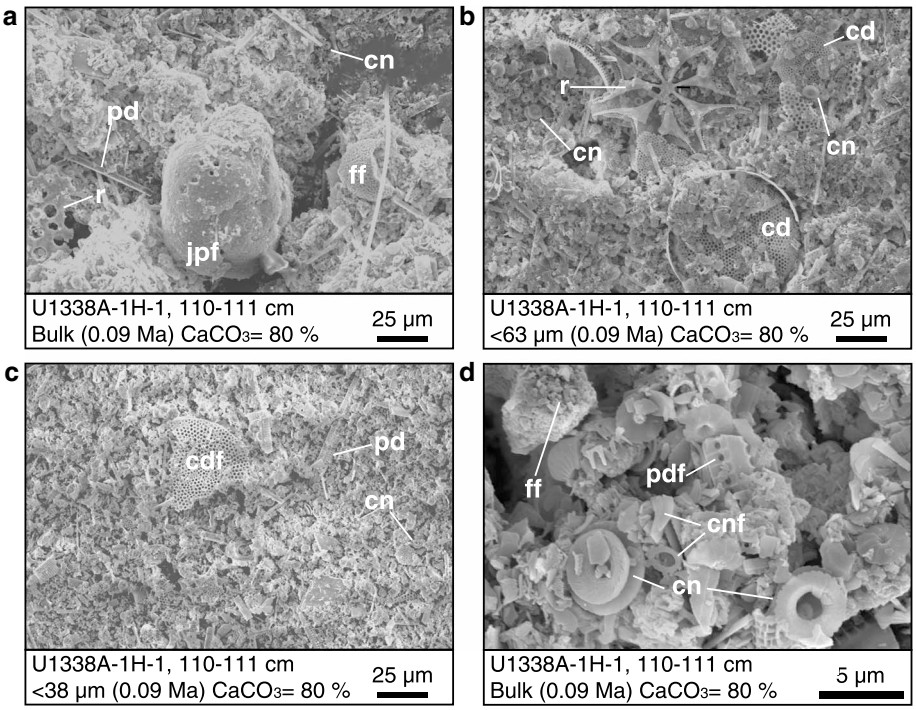

Figure 11. ESEM micrographs showing different components of (a) bulk, (b) <63 µm, and (c) <38 µm sediment and (d) the carbonate preservation in sample U1338A-1H-1, 110–111 cm. The magnification for Figures 11a–11c is 1000X, whereas the magnification of Figure 11d is 8000X. cd = centric diatom, cdf = centric diatom fragment, cn = calcareous nannofossil, cnf = calcareous nannofossil fragment, ff = foraminifera fragment, jpf = juvenile planktic foraminifera, pd = pennate diatom, pdf = pennate diatom fragment, r = radiolarian.

6.2. Grain Size Variability and Its Influence on Stable Isotope Compositions

Bulk carbonate in sediment beneath open ocean environments mostly consists of calcareous nannofossils and planktic foraminifera tests, including their fragments (Figure 11) [*McIntyre and McIntyre*, 1971; *Boeckel and Baumann*, 2004; *Frenz et al*., 2005; *Broecker and Clark*, 2009]. These biogenic carbonate components carry different $\delta^{13}C$ and $\delta^{18}O$ signatures depending on the calcification depth in the water column, the depth of the mixed layer, the biology of the living organism, and the season in which they calcify [*Curry et al*., 1983; *Spero*, 1998; *Kucera*, 2007; and the aforementioned references regarding calcareous nannoplankton]. Benthic foraminifera can also represent a small but significant fraction of the total carbonate in sediment, particularly at locations beneath the lysocline [*Conan et al*., 2002; *Hayward et al*., 2002], such as the case across much of the EEP. The stable isotope composition of bulk carbonate should thus represent an integrated

Table 4. Main Sediment Contributors of Figure 11 ESEM Micrographs

Sample	Sediment Fraction	Magnification	Sediment Components
U1338A-1H-1, 110–111 cm	Bulk	1000X	Juvenile planktic foraminifera, fragments of foraminifera test, diatom and radiolarian tests, pennate diatom tests, calcareous nannofossils groundmass
	<63 µm	1000X	Radiolarion test, centric diatom test, fragments of diatom and radiolarian tests, groundmass of calcareous nannofossils and siliceous microfossils fragments
	<38 µm	1000X	Fragment of centric diatom test, pennate diatom test, groundmass of calcareous nannofossils and siliceous microfossils fragments
	Bulk	8000X	Calcareous nannofossils, fragment of foraminifera test, fragments of calcareous nannofossils, fragment of pennate diatom test

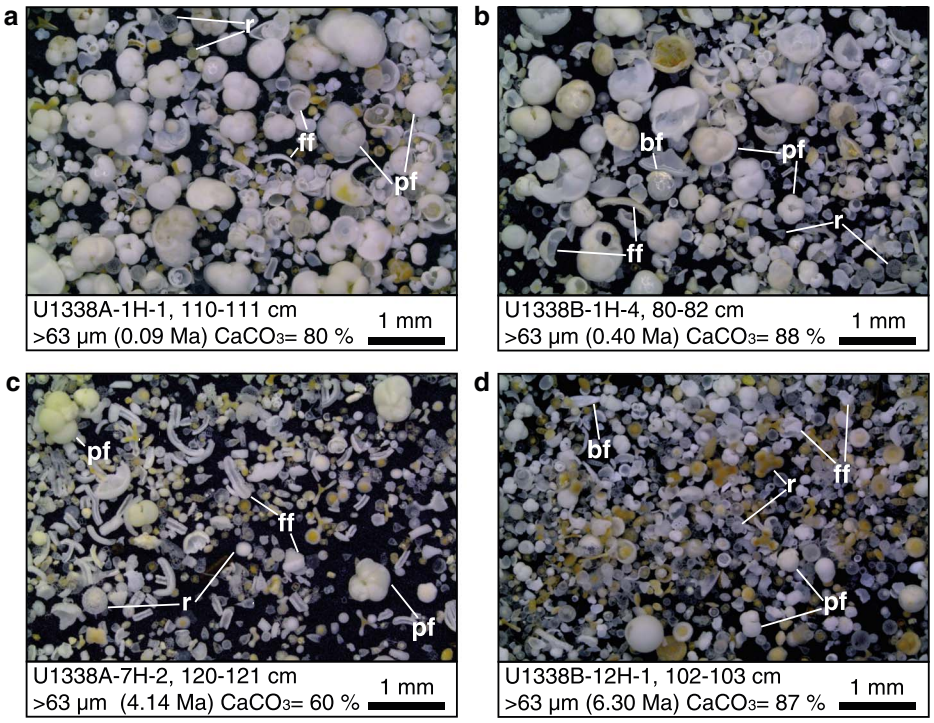

Figure 12. Reflected light micrographs showing the composition of the coarse fraction (>63 µm) in four representative sediment samples from Site U1338. bf = benthic foraminifera, ff = foraminifera fragment, pf = planktic foraminifera, r = radiolarian. Note that the main components of this size fraction are planktic foraminifera (calcareous) and radiolarians (siliceous). Proportions of these two main components vary between samples. In the two shallowest samples (Figures 12a and 12b), the coarse fraction is dominated by deep-dwelling species of planktic foraminifera such as *Globorotalia menardii*, *Globorotalia tumida*, and *Neogloboquadrina dutertrei*. In general, there are more radiolarians in older sediments (Figures 12c and 12d). Elongate segments of broken *Globorotalia* "keels" are very common foraminifera fragments of this size fraction.

signal of these calcareous components. The prediction is that <63 µm and <38 µm sediment fractions should be dominated increasingly by calcareous nannofossil carbonate [*Broecker and Clark*, 1999, 2009; *Frenz et al*., 2005] and, thus, should have a different stable isotope composition than bulk carbonate. One might also expect nannofossils on their own to record a dominantly mixed layer ocean signal, whereas the mixed species planktic foraminifera component might include a bias toward colder and deeper waters because of the broader spectrum of vertical depth habits occupied by tropical foraminifera [*Ennyu et al*., 2002; *Birch et al*., 2013].

At both Sites U1338 and 573, and for sediment deposited prior to approximately 4.4 Ma, there are virtually no differences in the $\delta^{13}C$ and $\delta^{18}O$ compositions between bulk carbonate and the <63 and <38 µm size fractions (Figure 10). The three fractions begin to diverge in sediment samples deposited after 4.4 Ma. For this younger time interval, bulk carbonate $\delta^{13}C$ values are slightly greater than the two fine fractions at both sites, while bulk carbonate $\delta^{18}O$ values are noticeably greater than the two fine fractions at Site U1338. Importantly, this separation of stable isotope composition by grain size coincides with a marked increase in the abundance of coarse (>63 µm) material. The coarse fraction increases from an average of 2 to 3% in sediment deposited before 4.4 Ma to an average of 10 to 11% in sediment deposited after 4.4 Ma.

The difference in stable isotope signals spanning our size-sorted isolates is interpreted to reflect changes in foraminiferal abundance. The amount of foraminiferal material in coarse fraction samples from Site U1338 increases with decreasing age of sediments at the expense of biosilica (Figure 12) [*Reghellin et al*., 2013]. More specifically, foraminifera are nearly absent from sediment deposited before 4.4 Ma but typically represent between 8 and 15% of bulk sediment deposited after 4.4 Ma (Table 2). For a sample with 10–11% coarse fraction, its bulk $\delta^{13}C$ is on average 0.17–0.22‰ greater than the $\delta^{13}C$ of the identical sample with most foraminiferal material removed (i.e., the <63 and <38 µm size fractions).

Irrespective of details, our results, combined with those of *Shackleton and Hall* [1995], suggest that foraminiferal carbonate has limited influence on bulk carbonate $\delta^{13}C$ and $\delta^{18}O$ profiles within the EEP. This is because bulk carbonate within the region mostly comprises calcareous nannofossils. The latter point is consistent with previous work [*Broecker and Clark*, 2009; *Lyle et al*., 2010], as well as our ESEM observations of bulk sediment (Figures 11 and S1–S3).

6.3. Stable Isotope Records of Calcareous Nannofossils Within the EEP

The stable isotope records of bulk carbonate at sites across the EEP are, almost assuredly, representing changes in the $\delta^{13}C$ and $\delta^{18}O$ composition of calcareous nannofossils. One issue is whether these records reflect, in part or at least for certain time intervals, significant recrystallization of calcareous nannofossils at or beneath the seafloor. Our ESEM observations (Figures 11 and S1–S3) reveal that foraminiferal fragments are highly dissolved and recrystallized; however, both placoliths and discoasters, which comprise most of the nannofossil carbonate, are intact and without obvious signs of extensive recrystallization or calcite overgrowth (Figure 11d), consistent with previous observations [*Pälike et al*., 2010; *Backman et al*., 2013]. The notion of limited nannofossil recrystallization in our samples makes sense. If the calcareous nannofossil component carrying the stable isotope signal was heavily modified near the seafloor, it should have a $\delta^{18}O$ value similar to that of benthic foraminifera [*Schrag et al*., 1995]. However, this is not the case, as benthic foraminifera in the EEP over the last 8 Ma have $\delta^{18}O$ values of 3 to 5‰ [*Mix et al*., 1995a, 1995b; *Shackleton et al*., 1995b]. Moreover, a major difference in $\delta^{18}O$ records with respect to site latitude (Figure 2) should not exist because bottom water temperature does not vary appreciably across the EEP. Significant carbonate recrystallization close to the seafloor can be ruled out further by the temporal coherency in $\delta^{13}C$ and $\delta^{18}O$ records at sites along the equator (Figures 7 and 9). Diagenetic modification of stable isotope signals, particularly $\delta^{18}O$, should occur with burial depth [*Schrag et al*., 1995; *Frank et al*., 1999], so that records would not align at sites with significantly different sedimentation rates (Figure 10).

As will become obvious below, it is also important to ask whether intervals marked by high $\delta^{18}O$ in bulk and fine-grained carbonate represent significant dissolution of phases with low $\delta^{18}O$. Beyond the aforementioned points, there exist basic relationships between bulk carbonate $\delta^{18}O$, bulk sediment carbonate content, and sedimentation rates. Over the long records (Figure 10) and over short depth intervals (Figure 8), samples with higher $\delta^{18}O$ generally have higher carbonate content. This observation is opposite to that expected for preferential dissolution of components depleted in ^{18}O but is consistent with enhanced carbonate production and preservation in the EEP during time intervals with colder surface water [Farrell and Prell, 1989; *Archer*, 1991].

A second issue is whether the stable isotope records might reflect temporal differences in the taxonomic profile of calcareous nannofossils [*Steinmetz*, 1994]. The late Miocene through Pleistocene calcareous nannofossil assemblages at both Sites 573 [*Pujos*, 1985a, 1985b] and U1338 [*Pälike et al*., 2010] are dominated by members of the phylomorphogenetic reticulofenestrid lineage (e.g., small reticulofenestrids, gephyrocapsids, *Pseudoemiliania lacunosa*, and *Emiliania huxleyi*). This taxonomic profile applies also to Sites 849, 850, and 852 [*Mayer et al*., 1992] and is important for two reasons. First, living modern examples of this lineage show maximum densities in the upper 100 m of the water column, including in the equatorial Pacific [*Honjo and Okada*, 1974]. Second, while various Holocene coccolithophores generate calcite with a wide range of stable isotope compositions from similar water, this variability becomes much smaller when examining certain "groups." Indeed, coccolithophores can be classified into groups on the basis of their $\delta^{18}O$ signatures, the reticulofenestrid lineage being one of them [*Dudley et al*., 1986; *Steinmetz*, 1994; *Hermoso et al*., 2014].

Despite the fact that nannofossil assemblages do not precipitate their calcite in equilibrium, *Steinmetz* [1994] notably suggested the $\delta^{18}O$ of sediment assemblages "reflected the temperature and isotopic ratio of the (mixed layer) water in which the coccolithophores had lived." This key conclusion was based on observed oxygen isotope covariations between planktic foraminiferal and nannofossil carbonate [*Anderson and Cole*, 1975; *Margolis et al*., 1975], including especially across a series of glacial-interglacial cycles (0–500 ka) in the classic P6304-4 core from the Caribbean [*Emiliani*, 1972; *Anderson and Steinmetz*, 1983]. Carbonate in this core is dominated by polyspecific members of the reticulofenestrid lineage, but *Steinmetz and Anderson* [1984] remarked that if "there are any species-dependent isotopic effects, their influence is not apparent."

In summary, stable isotope records of carbonate at Sites 573, U1338, and 850, in both bulk sediment and fine fractions and from the late Miocene to recent, represent an integrated signal dominated by the phylomorphogenetic reticulofenestrid lineage.

6.4. Understanding the Bulk Carbonate Stable Isotopes From a Paleoceanographic Perspective

In the modern EEP, most coccolithophores, especially including *Gephyrocapsa oceanica* and *E. huxleyi*, live and calcify within 100 m of the sea surface [*Hagino et al*., 2000]. For example, a study conducted during August–October 1969 and along 155°W longitude showed that, within 10° of the equator, concentrations of coccospheres in the water column were highest at about 50 m water depth, and they were an order of magnitude greater between 0 and 100 m water depth than between 100 and 200 m water depth [*Honjo and Okada*, 1974], a critical observation that is coherent with data from the equatorial Atlantic [*Bishop et al*., 1977].

The simplest explanation for our findings is that bulk carbonate stable isotope records along the equator, at least since 8 Ma, are tracking both long-term and short-term changes in coccolith calcite and hence corresponding variations in surface water conditions that impact this calcification. This view is consistent with early work on the topic from other regions [*Anderson and Steinmetz*, 1981, 1983; *Steinmetz*, 1994]. Such mixed layer variability might be expected to generate changes in bulk sediment composition. This is the case, as displayed by changes in sedimentation rates, coarse fraction percentages, and carbonate content at Sites U1338 and 573 (Figures 6 and 8), as well as decimeter-scale changes in sediment color and physical properties at many EEP sites [*Farrell et al*., 1995a; *Pisias et al*., 1995; *Lyle et al*., 2010; *Lyle and Backman*, 2013; *Reghellin et al*., 2013].

Having established that bulk carbonate $\delta^{13}C$ and $\delta^{18}O$ records probably reflect surface ocean conditions, we can hypothesize on processes that generated the signals. The first puzzle to explain is the similarity in the $\delta^{13}C$ records. Variations in bulk carbonate $\delta^{13}C$ appear to correlate across the EEP with less than 0.5‰ difference at any particular time, irrespective of whether the record comes from an on-equator site or an off-equator site (Figures 2 and 7). This suggests similar surface water carbon chemistry through time and more specifically that the $\delta^{13}C$ of dissolved inorganic carbon (DIC) coherently varied over a broader region than the focused zone of equatorial wind-driven upwelling.

A reasonable explanation for the common $\delta^{13}C$ signal comes from measurements and modeling of the $\delta^{13}C$ of DIC in present-day surface waters of the EEP [*Kroopnick*, 1985; *Gruber et al*., 1999; *Tagliabue and Bopp*, 2008]. Wind-driven upwelling brings ^{13}C-depleted DIC (and nutrients) into surface waters along the equator. However, the $\delta^{13}C$ of mixed layer DIC also depends on primary productivity, gas exchange with the atmosphere, and temperature. The consequence is an EEP with fairly diffuse gradients (~0.5‰) in the $\delta^{13}C$ of surface water DIC [*Lynch-Stieglitz et al*., 1995; *Tagliabue and Bopp*, 2008]. One might speculate that the coherent bulk carbonate $\delta^{13}C$ records across the EEP are providing information on past changes in factors that impact the modern $\delta^{13}C$ of surface water DIC in the region.

The second puzzle to solve is the absolute value of bulk carbonate $\delta^{13}C$. Uppermost sediment samples at sites across the EEP consistently have bulk carbonate $\delta^{13}C$ compositions between 0.3 and 0.6‰ (Figures 2 and 7). These values appear to drop by about 0.4‰ after sieving and removal of foraminifera (Figure 10). It is often stated that coccolithophores precipitate calcite from HCO_3^- (as summarized and discussed by *Paasche* [2001]). However, the $\delta^{13}C$ of modern DIC in the upper 100 m of surface waters above our sites (after correcting for the "Suess effect") ranges between 1.0 and 1.3‰ [*Kroopnick*, 1985; *Gruber et al*., 1999; *Tagliabue and Bopp*, 2008], and carbon isotope fractionation during calcite precipitation at 25°C should *increase* these values by about 1.0 to 1.6‰ [*Emrich et al*., 1970; *Romanek et al*., 1992; *Zhang et al*., 1995; *Zeebe et al*., 1999]. In short, average $\delta^{13}C$ values of bulk carbonate in uppermost samples are too "light" by at least 2.0‰ if calcite precipitation occurred in equilibrium with HCO_3^-.

Much of the answer probably lies in biochemistry. However, an exact reason is not clear because of differing views as how the reticulofenestrid lineage precipitate their coccoliths. Various experiments suggest that modern coccolithophores take HCO_3^- through the cell wall into "coccolith vesicles," the microenvironments where calcite precipitation occurs [*Paasche*, 2001]. One view is that, within these vesicles, pH is modified through the release of H^+ to chloroplasts, where the H^+ increases CO_2 available for photosynthesis [*Anning*

et al., 1996; *Buitenhuis et al*., 1999; *Paasche*, 2001]. Calcite thus precipitates within coccolith vesicles at an elevated pH and dominantly from CO_3^{2-} (above references). At 25°C, this should significantly decrease the $\delta^{13}C$ of calcite relative to that expected from DIC [*Zeebe et al*., 1999], perhaps by about 2.0‰ [*Zhang et al*., 1995]. While this pathway likely operates for certain (generally larger) coccolithophore species, *Rickaby et al*. [2010] suggest this is not the case for the reticulofenestrid lineage, because their coccoliths have a similar $\delta^{13}C$ composition to that of the surrounding DIC. In these experiments, however, the $\delta^{13}C$ of the DIC increased over time (presumably because of removal of organic carbon), and there is no accounting for the fractionation between DIC and calcite. Most recently, *Hermoso* [2015] has indicated that the carbon comes into an internal pool as aqueous CO_2, and the end $\delta^{13}C$ of calcite depends on growth rate (organic carbon production), coccolith size, and aqueous CO_2 concentrations. Our data do not really address this topic, although we stress that a remarkably similar $\delta^{13}C$ signal is found across the EEP (Figures 2 and 7), which would suggest that, despite biochemistry complexities, a coherent signal emerges.

Such an explanation leads to a third puzzle: the absolute value of bulk carbonate $\delta^{18}O$. Modern surface water above Sites U1338 and 573 has average multiannual temperatures of about 26°C (Figure 1 [*Johnson et al*., 2002]) and average $\delta^{18}O$ values of about 0.4‰ [*Schmidt et al*., 1999; *LeGrande and Schmidt*, 2006]. Over the upper 100 m of water across the general region, temperature decreases by 4 to 8°C, depending on location [*Johnson et al*., 2002], while the $\delta^{18}O$ of water ($\delta^{18}O_w$) typically remains within 0.2‰ [*Schmidt et al*., 1999]. At both sites and at 50 m water depth—the approximate horizon of maximum coccolithophore abundance [*Honjo and Okada*, 1974]—average temperatures are 25°C.

The relationship between temperature, $\delta^{18}O_w$, and the $\delta^{18}O$ of calcite ($\delta^{18}O_c$) can be predicted through a widely referenced equation [*Kim and O'Neil*, 1997], as modified by *Bemis et al*. [1998]:

$$T\,(°C) = 16.1 - 4.64 \bullet \left(\delta^{18}O_c\text{-}\delta^{18}O_w\right) + 0.09 \bullet \left(\delta^{18}O_c\text{-}\delta^{18}O_w\right)^2. \quad (1)$$

Considering a temperature of 25°C and a $\delta^{18}O_w$ of 0.4‰, carbonate in uppermost samples at Sites U1338 and 573 should have $\delta^{18}O$ compositions of nominally −1.2‰. This is not the case (Figures 9 and 10). Sieving sediment at these sites partly addresses the discrepancy, as it removes large grains of carbonate enriched in ^{18}O (Figure 12). Recall that our sites lie below the lysocline, so that foraminifer assemblages are dominated by "deep-dwelling" species (e.g., *Globorotalia tumida*; Figure 12), which have tests enriched in ^{18}O relative to bulk sediment [*Farrell et al*., 1995b; *Cannariato and Ravelo*, 1997]. Nonetheless, fine-grained carbonate in the uppermost sediment at Sites U1338 and 573 has a $\delta^{18}O$ composition about 1‰ greater than expected for equilibrium calcite.

As with $\delta^{13}C$, pH and the distribution of carbonate species impacts the $\delta^{18}O$ of precipitated calcite [*Zeebe*, 2007]. The internal regulation of chemistry by coccolithophores might, therefore, modify $\delta^{18}O$ values of calcite relative to those expected from ambient temperature and $\delta^{18}O_w$. For members of the reticulofenestrid lineage grown in culture experiments and isolated from core top sediment, especially *G. oceanica*, there is a nominally 1‰ increase in $\delta^{18}O$ relative to that expected for calcite [*Dudley et al*., 1986; *Steinmetz*, 1994; *Ziveri et al*., 2003]. With this offset, the sieved uppermost samples at Sites U1338 and 573 render SSTs of ~25°C. This is consistent with the idea that the $\delta^{18}O$ of calcite precipitated by various coccolithophores strongly depends on temperature [*Dudley and Goodney*, 1979; *Dudley et al*., 1980, 1986; *Ziveri et al*., 2003; *Rickaby et al*., 2010; *Candelier et al*., 2013].

All the above leads to the fourth, major puzzle requiring explanation. Our new data from Sites U1338 and 573 show low $\delta^{18}O$ values between 8 and 4 Ma in bulk sediment, as well as in the <63 μm and <38 μm sediment fractions (Figures 2, 9, and 10). The observation by *Shackleton and Hall* [1995] extends over a wide area along the Pacific equator. As discussed above, the low bulk carbonate $\delta^{18}O$ values probably do not result from variations in the composition of the biogenic carbonate size fractions and sublysocline carbonate dissolution. Indeed, the late Miocene through Pleistocene interval at Site U1338 is completely dominated by small-sized members of the reticulofenestrid lineage including *Gephyrocapsa ericsonii* (0–1.6 Ma), *P. lacunosa* (0.8–2.3 Ma), *Reticulofenestra haqii* (2.7–8 Ma), and *Dictyococcites* spp. <3 μm (1.8–8 Ma) [*Bolton et al*., 2010; *Pälike et al*., 2010; Figures S2d and S3d]. Instead, the simplest explanation is that the low bulk carbonate $\delta^{18}O$ values reflect colder mixed layer temperatures along the equator during the late Miocene and early Pliocene, which presumably would derive from enhanced wind-driven equatorial upwelling

[*Shackleton and Hall*, 1995]. Given modern relationships between wind-driven circulation, surface temperature, and primary productivity along the equator [*Pennington et al*., 2006], intensified upwelling of cold, nutrient-rich waters along the equator between 8 and 4 Ma would be consistent with significantly higher sedimentation rates of biogenic components at Sites U1338 and 573 (Figures 5 and 10) and at other sites along the equator of the EEP [*van Andel et al*., 1975; *Delaney and Filippelli*, 1994; *Farrell et al*., 1995a; *Pisias et al*., 1995; *Schroeder et al*., 1997; *Lyle*, 2003; *Lyle and Baldauf*, 2015]. In fact, higher sediment accumulation rates of biogenic components occurred at multiple regions of upwelling across the Indian and Pacific Oceans between nominally 8 and 4 Ma, a phenomenon coined the "biogenic bloom" [*Peterson and Backman*, 1990; *Farrell et al*., 1995a; *Dickens and Owen*, 1999; *Grant and Dickens*, 2002].

The problem with a scenario of strengthened upwelling of cold water along the Pacific equator between 8 and 4 Ma is that it seemingly conflicts with a common idea presented in the literature over the last 12 years or so. A series of studies focusing on late Neogene paleoceanography in the EEP [*Ravelo et al*., 2004; *Wara et al*., 2005; *Brierley et al*., 2009; *Steph et al*., 2010; *Ford et al*., 2015] have suggested higher SSTs and weakened wind-driven upwelling during the early Pliocene. One possibility for the divergent interpretations concerns the sediment material used to make such reconstructions. Carbonate accumulation rates across the EEP appear to have been more focused between 8 and 4 Ma relative to present day; more specifically, these rates were significantly higher during the late Miocene and early Pliocene at locations broadly coincident with the area of strong wind-driven upwelling (Figure 1) but not outside of this region [*van Andel et al*., 1975; *Farrell et al*., 1995a; *Lyle*, 2003]. Records generated from sites within or outside the area of high biogenic accumulation rates might, therefore, give contrasting views on past SST. Indeed, this may explain the major difference in bulk carbonate $\delta^{18}O$ records between on-equator and off-equator sites of the EEP during the late Miocene and early Pliocene (Figure 2). Several widely discussed records also terminate between 4 and 5 Ma, so that changes over the longer time remain unclear.

A second possibility is the complexity and diversity of proxies being used [*Dickens and Backman*, 2012; *Lea*, 2014]. We do not fully understand the incorporation of stable isotopes into coccoliths of a single species [*Ziveri et al*., 2003; *Rickaby et al*., 2010; *Candelier et al*., 2013], let alone bulk carbonate, which in the EEP mostly represents an agglomeration of coccoliths from multiple species. However, it is intriguing that recent TEX_{86} records from the EEP [*Seki et al*., 2012; *Zhang et al*., 2014] also suggest cool late Miocene and early Pliocene temperatures along the Pacific equator, a finding that further questions the accepted view of higher SSTs and weakened wind-driven circulation during this time. Given that a main argument for higher early Pliocene SSTs comes from Mg/Ca ratios of planktic foraminifera [*Wara et al*., 2005; *Ravelo*, 2010; *Steph et al*., 2010; *Ford et al*., 2015], it is worth considering the validity of this proxy in regions characterized by strong but variable upwelling over time. Increased upwelling should lower the pH of the mixed layer, which would increase the Mg/Ca ratio of planktic foraminifera significantly [*Lea et al*., 1999]. Thus, there can be an inferred increase in SST using this proxy when the opposite actually occurred [*Dickens and Backman*, 2012]. Superimposed on this issue are the dynamics of the EEP region. Clearly, large amplitude variations in sediment properties and chemistry happened over very short increments of time and depth (Figure 8). With most paleoceanographic records from the region, it is not clear either how various measurements align in detail nor how they might be affected by temporal variability in surface water properties.

7. Conclusions

This study attempts to improve the understanding of bulk carbonate stable isotopes for paleoceanographic reconstructions. The comparison of our new data from Sites U1338 and 573 with data from Leg 138 sites [*Shackleton and Hall*, 1995] permits us to answer the initially posed four questions:

1. Are the published bulk carbonate $\delta^{13}C$ and $\delta^{18}O$ records coherent across a wide distance along the Pacific equator? The new bulk sediment stable isotope records at Sites U1338 and 573 show that similar records extend over 2500 km.
2. Are the published records masking much finer centimeter- to decimeter-scale variability in stable isotopes? Comparison of the new and published records based on discrete 1 to 3 cm depth-interval samples shows that the existing data sets from ODP Leg 138 are integrating short-term variability. This dampened variability likely reflects the sampling method used previously, in which each sample represents the homogenization of short-term (10–100 ka) changes in stable isotope composition over typically 150 cm long core sections.

3. Are the bulk carbonate records predominantly reflecting the $\delta^{13}C$ and $\delta^{18}O$ composition of the calcareous nannofossil component and therefore a surface mixed layer signal? The absence of major differences between the stable isotope compositions of bulk sediment and the <63 μm and <38 μm sediment fractions indicates that the stable isotope composition of bulk carbonate dominantly represents that of calcareous nannofossils. This is confirmed by the low amounts of coarse fraction determined for bulk sediment and direct observations of bulk sediment. The lower $\delta^{13}C$ and $\delta^{18}O$ values of the <63 μm and <38 μm fractions in sediment younger than 4.4 Ma can be explained by differential carbonate dissolution, which has the effect of increasing the content of deep-dwelling planktic foraminifera calcite (enriched in ^{18}O) in bulk carbonate and shifting the bulk toward higher values. However, alteration of bulk carbonate $\delta^{13}C$ and $\delta^{18}O$ by differential carbonate dissolution and preservation appears to be minimal, because calcareous nannofossils at Site U1338 do not show signs of extensive recrystallization over the last 8 Ma.
4. Are variations in stable isotopes, both long-term and short-term, coupled to changes in the biogenic composition of sediment? Variations of bulk carbonate $\delta^{13}C$ and $\delta^{18}O$ over the last 8 Ma are coupled to changes in the biogenic composition of sediment as indicated by correlative changes in sediment color, physical properties, sedimentation rates, carbonate content, and coarse fraction percentage.

The Earth science community is generally aware as to how diagenesis and lithification affect stable isotope signals of bulk marine sediment [*Schrag et al.*, 1995; *Frank et al.*, 1999]. Ironically, it seems less clear as to how bulk marine sediment acquires its stable isotope signal in the first place. In pursuing the above basic questions regarding bulk sediment stable isotopes and bulk sediment accumulation within the EEP from a deep-time perspective, we have tapped into far better and far more interesting avenues of future research.

The absolute values of bulk sediment $\delta^{13}C$ and $\delta^{18}O$ in the EEP are possibly close to that expected from equilibrium calculations for stable isotopes if most coccolithophores in this region internally regulate pH and principally use CO_3^{2-} to precipitate their coccoliths. This is not a novel idea [*Anning et al.*, 1996; *Buitenhuis et al.*, 1999; *Rickaby et al.*, 2010; *Candelier et al.*, 2013]. Beyond culturing experiments, however, the concept might be tested further by examining the $\delta^{13}C$ and $\delta^{18}O$ of bulk sediment, fine-grained sediment fractions, and microfiltered species-specific coccoliths from cores across the broad EEP, where temperature and DIC $\delta^{13}C$ varies significantly with latitude and longitude.

The similar bulk carbonate $\delta^{13}C$ records across most of the EEP since 8 Ma suggest covarying changes in $\delta^{13}C$ and concentrations of DIC within surface waters of this region throughout the late Neogene. Such temporal covariance is not unexpected given the modern diffuse gradients in $\delta^{13}C$ of surface water DIC [*Kroopnick*, 1985; *Tagliabue and Bopp*, 2008]. However, the precise timing and cause of these $\delta^{13}C$ changes, which exceed 2‰, are not clear. High-resolution $\delta^{13}C$ records are needed from multiple EEP sites.

The high $\delta^{18}O$ values in bulk carbonate along the Pacific equator during the late Miocene and early Pliocene, especially in conjunction with higher biogenic sediment accumulation rates, commands attention. With available information, there seems to be a major discrepancy in paleoceanographic interpretations derived from planktic foraminifera. Given the remarkable short-term changes in sediment composition within the EEP, an obvious step forward would be to generate a range of stable isotope records (bulk, fine fraction, and foraminifera), as well as other proxies for temperature and carbon cycling, in the same samples from multiple locations.

Acknowledgments
We thank Ted Moore, Paul Wilson and an anonymous reviewer for constructive input, which helped improving this manuscript. We are grateful to Klara Hajnal, Carina Johansson, and Laura Martinez for sample preparations and to Heike Siegmund for mass spectrometer analyses. We thank the Integrated Ocean Drilling Program for providing the samples. All data presented in this study are available at http://bolin.su.se/data/Reghellin-2015. This study was supported by the Swedish Research Council and Stockholm University.

References

Anderson, T. F., and S. A. Cole (1975), The stable isotope geochemistry of marine coccoliths: A preliminary comparison with planktonic foraminifera, *J. Foraminiferal Res.*, *5*, 188–192.
Anderson, T. F., and J. C. Steinmetz (1981), Isotopic and biostratigraphical records of calcareous nannofossils in a Pleistocene core, *Nature*, *294*, 24–31.
Anderson, T. F., and J. C. Steinmetz (1983), Stable isotopes in calcareous nannofossils: Potential application to deep-sea paleoenvironmental reconstructions during the Quaternary, *Utrecht Micropaleontol. Bull.*, *30*, 189–204.
Anning, T., N. A. Nimer, M. J. Merrett, and C. Brownlee (1996), Costs and benefits of calcification in coccolithophorids, *J. Mar. Syst.*, *9*, 45–56.
Archer, D. (1991), Equatorial Pacific calcite preservation cycles: Production or dissolution?, *Paleoceanography*, *6*, 561–571, doi:10.1029/91PA01630.
Arrhenius, G. (1952), Sediment cores from the East Pacific, *Rep. Swed. Deep-Sea Exped.*, *5*, 1–227.
Backman, J., I. Raffi, M. Ciummelli, and J. Baldauf (2013), Species-specific responses of late Miocene *Discoaster* spp. to enhanced biosilica productivity conditions in the equatorial Pacific and the Mediterranean, *Geo Mar. Lett.*, *33*, 285–298.
Baldauf, J. G. (1985), A high resolution late Miocene-Pliocene diatom biostratigraphy for the eastern equatorial Pacific, in *Proceedings of the Deep Sea Drilling Project*, *Init. Rep.*, vol. 85, edited by L. Mayer et al., pp. 457–475, U.S. Govt. Print. Off., Wash.

Baldauf, J. G. (2013), Data report: Diatoms from Sites U1334 and U1338, Expedition 320/321, in *Proceedings of the Integrated Ocean Drilling Program*, vol. 320/321, edited by H. Pälike et al., IODP Manage. Int., Inc., Tokyo, doi:10.2204/iodp.proc.320321.215.2013.
Baldauf, J. G., and M. Iwai (1995), Neogene diatom biostratigraphy for the eastern equatorial Pacific Ocean, Leg 138, in *Proceedings of the Ocean Drilling Program, Sci. Results*, vol. 138, edited by N. G. Pisias et al., pp. 105–128, Ocean Drilling Program, College Station, Tex.
Barber, R. T., and F. P. Chavez (1986), Ocean variability in relation to living resources during the 1982/83 El Niño, *Nature*, *319*, 279–285.
Barron, J. A. (1985), Diatom paleoceanography and paleoclimatology of the central and eastern equatorial Pacific between 18 and 6.2 Ma, in *Proceedings of the Deep Sea Drilling Project*, *Init. Rep*., vol. 85, edited by L. Mayer et al., pp. 935–945, Deep Sea Drilling Project, Wash.
Bemis, B. E., H. J. Spero, J. Bijma, and D. W. Lea (1998), Reevaluation of the oxygen isotope composition of planktonic foraminifera: Experimental results and revised paleotemperature equations, *Paleoceanography*, *13*, 150–160, doi:10.1029/98PA00070.
Berger, W. H. (1973a), Deep-sea carbonates: Pleistocene dissolution cycles, *J. Foraminiferal Res.*, *3*, 187–195.
Berger, W. H. (1973b), Cenozoic sedimentation in the eastern tropical Pacific, *Geol. Soc. Am. Bull.*, *84*, 1941–1954.
Berger, W. H. (1979), Preservation of foraminifera, in *Foraminiferal Ecology and Paleoecology*, *SEPM Short Course*, vol. 6, edited by J. Lipps et al., pp. 105–155, Soc. of Econ. Paleontol. and Mineral., Houston, Tex.
Bergreen, W. A., D. V. Kent, C. C. Swisher, and M. P. Aubry (1995), A revised Cenozoic geochronology and chronostratigraphy, *Geochronology Time Scales and Global Stratigraphic Correlation*, *SEPM Spec. Publ., 54*, 129–212.
Birch, H., H. K. Coxall, P. N. Pearson, D. Kroon, and M. O'Regan (2013), Planktonic foraminifera stable isotopes and water column structure: Disentangling ecological signals, *Mar. Micropaleontol.*, *101*, 127–145.
Bishop, J. K. B., J. M. Edmond, D. R. Ketten, M. P. Bacon, and W. B. Silker (1977), The chemistry, biology, and vertical flux of particulate matter from the upper 400 m of the equatorial Atlantic Ocean, *Deep Sea Res.*, *24*, 511–548.
Blaj, T., J. Backman, and I. Raffi (2009), Late Eocene to Oligocene preservation history and biochronology of calcareous nannofossils from paleo-equatorial Pacific Ocean sediments, *Riv. Italiana Paleontol. Stratigrafia*, *115*, 67–85.
Bloomer, S. F., and L. A. Mayer (1997), Core-log-seismic integration as a framework for determining the basin-wide significance of regional reflectors in the eastern equatorial Pacific, *Geophys. Res. Lett.*, *24*, 321–324, doi:10.1029/96GL02076.
Boeckel, B., and K. H. Baumann (2004), Distribution of coccoliths in surface sediments of the south-eastern South Atlantic Ocean: Ecology, preservation and carbonate contribution, *Mar. Micropaleontol.*, *51*, 301–332.
Bolton, C. T., and H. M. Stoll (2013), Late Miocene threshold response of marine algae to carbon dioxide limitation, *Nature*, *500*, 558–562.
Bolton, C. T., S. J. Gibbs, and P. A. Wilson (2010), Evolution of nutricline dynamics in the equatorial Pacific during the late Pliocene, *Paleoceanography*, *25*, PA1207, doi:10.1029/2009PA001821.
Bolton, C. T., H. M. Stoll, and A. Mendez-Vicente (2012), Vital effects in coccolith calcite: Cenozoic climate-*p*CO2 drove the diversity of carbon acquisition strategies in coccolithophores?, *Paleoceanography*, *27*, PA4204, doi:10.1029/2012PA002339.
Boudreau, B. P., J. J. Middelburg, and F. J. Meysman (2010), Carbonate compensation dynamics, *Geophys. Res. Lett.*, *37*, L03603, doi:10.1029/2009GL041847.
Brierley, C. M., A. V. Fedorov, Z. Liu, T. D. Herbert, K. T. Lawrence, and J. P. LaRiviere (2009), Greatly expanded tropical warm pool and weakened Hadley circulation in the early Pliocene, *Science*, *323*, 1714–1718.
Broecker, W. S., and E. Clark (1999), $CaCO_3$ size distribution: A paleocarbonate ion proxy?, *Paleoceanography*, *14*, 596–604, doi:10.1029/1999PA900016.
Broecker, W. S., and E. Clark (2009), Ratio of coccolith $CaCO_3$ to foraminifera $CaCO_3$ in late Holocene deep sea sediments, *Paleoceanography*, *24*, PA3205, doi:10.1029/2009PA001731.
Buitenhuis, E., H. J. W. de Baar, and M. J. W. Vedhuis (1999), Photosynthesis and calcification by *Emiliania huxleyi* (Prymnesiophyceae) as a function of inorganic carbon, *J. Phycol.*, *35*, 949–959.
Candelier, Y., F. Minoletti, I. Probert, and M. Hermoso (2013), Temperature dependence of oxygen isotope fractionation in coccolith calcite: A culture and core top calibration of the genus *Calcidiscus*, *Geochim. Cosmochim. Acta*, *100*, 264–281.
Cannariato, K. G., and A. C. Ravelo (1997), Pliocene-Pleistocene evolution of eastern tropical Pacific surface water circulation and thermocline depth, *Paleoceanography*, *12*, 805–820, doi:10.1029/97PA02514.
Chavez, F. P., and R. T. Barber (1987), An estimate of new production in the equatorial Pacific, *Deep Sea Res.*, *34*, 1229–1243.
Conan, S. M. -H., E. M. Ivanova, and G.-J. A. Brummer (2002), Quantifying carbonate dissolution and calibration of foraminiferal dissolution indices in the Somali Basin, *Mar. Geol.*, *182*, 325–349.
Curry, W. B., R. C. Thunell, and S. Honjo (1983), Seasonal changes in the isotopic composition of planktonic foraminifera collected in Panama Basin sediment traps, *Earth Planet. Sci. Lett.*, *64*, 33–43.
Delaney, M. L., and G. M. Filippelli (1994), An apparent contradiction in the role of phosphorus in Cenozoic chemical mass balances for the world ocean, *Paleoceanography*, *9*, 513–527, doi:10.1029/94PA00795.
Dickens, G. R., and J. Backman (2012), A comment on "Pliocene climate change of the Southwest Pacific and the impact of ocean gateways", *Earth Sci. Planet. Lett.*, *331–332*, 364–365.
Dickens, G. R., and R. M. Owen (1999), The latest Miocene-early Pliocene biogenic bloom: A revised Indian Ocean perspective, *Mar. Geol.*, *161*, 75–91.
Dudley, W. C., and D. E. Goodney (1979), Oxygen isotope content of coccoliths grown in culture, *Deep Sea Res.*, *26*, 495–503.
Dudley, W. C., and C. S. Nelson (1988), The $\delta^{13}C$ content of calcareous nannofossils as an indicator of Quaternary paleoproductivity in the southwest Pacific region, *N. Z. J. Geol. Geophys.*, *31*, 111–116.
Dudley, W. C., J. C. Duplessy, P. L. Blackwelder, L. E. Brand, and R. R. L. Guillard (1980), Coccoliths in Pleistocene-Holocene nannofossil assemblages, *Science*, *285*, 222–223.
Dudley, W. C., P. Blackwelder, L. Brand, and J. C. Duplessy (1986), Stable isotope compositions of coccoliths, *Mar. Micropaleontol.*, *10*, 1–8.
Dunn, D. A. (1982), Change from "Atlantic-type" to "Pacific-type" carbonate stratigraphy in the middle Pliocene equatorial Pacific Ocean, *Mar. Geol.*, *50*, 41–60.
Emiliani, C. (1955), Pleistocene temperatures, *J. Geol.*, *63*, 538–578.
Emiliani, C. (1972), Quaternary paleotemperatures and the duration of the high-temperature intervals, *Science*, *178*, 398–401.
Emrich, K., D. H. Ehhalt, and J. C. Vogel (1970), Carbon isotope fractionation during the precipitation of calcium carbonate, *Earth Sci. Planet. Lett.*, *8*, 363–371.
Ennyu, A., M. A. Arthur, and M. Pagani (2002), Fine-fraction carbonate stable isotopes as indicators of seasonal shallow mixed-layer paleohydrography, *Mar. Micropaleontol.*, *46*, 317–342.
Farrell, J. W., and W. L. Prell (1989), Climatic change and $CaCO_3$ preservation: An 800,000 years bathymetric reconstruction from the central equatorial Pacific Ocean, *Paleoceanography*, *4*, 447–466, doi:10.1029/PA004i004p00447.

Farrell, J. W., I. Raffi, T. R. Janecek, D. W. Murray, M. Levitan, K. A. Dadey, K. C. Emeis, M. Lyle, L. A. Flores, and S. Hovan (1995a), Late Neogene sedimentation patterns in the eastern equatorial Pacific Ocean, in *Proceedings of the Ocean Drilling Program, Sci. Results*, vol. 138, edited by N. G. Pisias et al., pp. 717–756, Ocean Drilling Program, College Station, Tex.

Farrell, J. W., D. W. Murray, V. S. McKenna, and A. C. Ravelo (1995b), Upper ocean temperature and nutrient contrasts inferred from Pleistocene planktonic foraminifer $\delta^{18}O$ and $\delta^{13}C$ in the eastern equatorial Pacific, in *Proceedings of the Ocean Drilling Program, Sci. Results*, vol. 138, edited by N. G. Pisias et al., pp. 289–319, Ocean Drilling Program, College Station, Tex.

Fiedler, P. C., V. Philbrick, and F. P. Chavez (1991), Oceanic upwelling and productivity in the eastern tropical Pacific, *Limnol. Oceanogr.*, *36*, 1834–1850.

Ford, H. L., A. C. Ravelo, P. S. Dekens, J. P. LaRiviere, and M. W. Wara (2015), The evolution of the equatorial thermocline and the early Pliocene *El Padre* mean state, *Geophys. Res. Lett.*, *42*, 4878–4887, doi:10.1002/2015GL064215.

Frank, T. D., M. A. Arthur, and W. E. Dean (1999), Diagenesis of Lower Cretaceous pelagic carbonates, North Atlantic: Paleoceanographic signals obscured, *J. Foraminiferal Res.*, *29*, 340–351.

Frenz, M., K. H. Baumann, B. Boeckel, R. Höppner, and R. Henrich (2005), Quantification of foraminifer and coccolith carbonate in South Atlantic surface sediments by means of carbonate grain-size distributions, *J. Sediment. Res.*, *75*, 464–475.

Gartner, S., and J. Chow (1985), Calcareous nannofossil biostratigraphy, Deep Sea Drilling Project Leg 85, eastern equatorial Pacific, in *Proceedings of the Deep Sea Drilling Project, Init. Rep.*, vol. 85, edited by L. A. Mayer et al., pp. 609–619, Deep Sea Drilling Project, Wash.

Goodney, D. E., S. V. Margolis, W. C. Dudley, P. Kroopnick, and D. F. Williams (1980), Oxygen and carbon isotopes of recent calcareous nannofossils as paleoceanographic indicators, *Mar. Micropaleontol.*, *5*, 31–42.

Graber, K. K., E. Pollard, B. Jonasson, and E. Schulte (2002), Overview of Ocean Drilling Program engineering tools and hardware, *Ocean Drill. Program Tech. Note*, *31*, doi:10.2973/odp.tn.31.2002.

Grant, K. M., and G. R. Dickens (2002), Coupled productivity and carbon isotope records in the southwest Pacific Ocean during the late Miocene-early Pliocene biogenic bloom, *Palaeogeogr. Palaeoclimatol. Palaeoecol.*, *187*, 61–82.

Gruber, N., C. D. Keeling, R. B. Bacastow, P. R. Guenther, T. J. Lueker, M. Wahlen, H. A. J. Meijer, W. G. Mook, and T. F. Stocker (1999), Spatiotemporal patterns of carbon-13 in the global surface oceans and the oceanic Suess effect, *Global Biogeochem. Cycles*, *13*, 307–335, doi:10.1029/1999GB900019.

Hagino, K., H. Okada, and H. Matsuoka (2000), Spatial dynamics of coccolithophores in the equatorial western-central Pacific Ocean, *Mar. Micropaleontol.*, *39*, 53–72.

Hayward, B. W., H. Neil, R. Carter, H. R. Grenfell, and J. J. Hayward (2002), Factors influencing the distribution patterns of recent deep-sea benthic foraminifera, east of New Zealand, Southwest Pacific Ocean, *Mar. Micropaleontol.*, *46*, 139–176.

Herbert, T., and L. A. Mayer (1991), Long climatic time series from sediment physical property measurements, *J. Sediment. Res.*, *61*, 1089–1108.

Hermoso, M. (2015), Control on ambient pH on growth and stable isotopes in phytoplanktonic calcifying algae, *Paleoceanography*, *30*, 1100–1112, doi:10.1002/2015PA002844.

Hermoso, M., T. J. Horner, F. Minoletti, and R. E. M. Rickaby (2014), Constraints on the vital effect in coccolithophore and dinoflagellate calcite by oxygen isotopic modification of seawater, *Geochim. Cosmochim. Acta*, *141*, 612–627.

Honjo, S., and H. Okada (1974), Community structure of coccolithophores in the photic layer of the mid-Pacific, *Micropaleontology*, *20*, 209–230.

Jarvis, I., A. S. Gale, H. C. Jenkyns, and M. A. Pearce (2006), Secular variation in Late Cretaceous carbon isotopes: A new $\delta^{13}C$ carbonate reference curve for the Cenomanian–Campanian (99.6–70.6 Ma), *Geol. Mag.*, *143*, 561–608.

Johnson, G. C., B. M. Sloyan, W. S. Kessler, and K. E. McTaggart (2002), Direct measurements of upper ocean currents and water properties across the tropical Pacific during the 1990s, *Prog. Oceanogr.*, *52*, 31–61.

Kessler, W. S. (2006), The circulation of the eastern tropical Pacific: A review, *Prog. Oceanogr.*, *69*, 181–217.

Killingley, J. S. (1983), Effects of diagenetic recrystallization on $^{18}O/^{16}O$ values of deep sea sediments, *Nature*, *301*, 594–596.

Kim, S.-T., and J. R. O'Neil (1997), Equilibrium and nonequilibrium oxygen isotope effects in synthetic carbonates, *Geochim. Cosmochim. Acta*, *61*, 3461–3475.

Kroopnick, P. M. (1985), The distribution of ^{13}C of ΣCO_2 in the world oceans, *Deep Sea Res., Part A*, *32*, 57–84.

Kucera, M. (2007), Planktonic foraminifera as tracers of past oceanic environments, *Dev. Mar. Geol.*, *1*, 213–262.

Lea, D. W. (2014), Not so permanent El Niño, *Science*, *344*, 52–53.

Lea, D. W., T. A. Mashiotta, and H. J. Spero (1999), Controls on magnesium and strontium uptake in planktonic foraminifera determined by live culturing, *Geochim. Cosmochim. Acta*, *63*, 2369–2379.

LeGrande, A. N., and G. A. Schmidt (2006), Global gridded data set of the oxygen isotopic composition in seawater, *Geophys. Res. Lett.*, *33*, L12604, doi:10.1029/2006GL026011.

Liu, C., X. Cheng, Y. Zhu, J. Tian, and P. Xia (2002), Oxygen and carbon isotope records of calcareous nannofossils for the past 1 Ma in the southern South China Sea, *Chin. Sci. Bull.*, *47*, 798–803.

Lourens, L. J., F. J. Hilgen, N. J. Shackleton, J. Laskar, and D. Wilson (2004), The Neogene period, in *A Geological Time Scale 2004*, edited by F. M. Gradstein, J. G. Ogg, and A. G. Smith, pp. 409–440, Cambridge Univ. Press, Cambridge, U. K.

Lourens, L. J., A. Sluijs, D. Kroon, J. C. Zachos, E. Thomas, U. Röhl, J. Bowles, and I. Raffi (2005), Astronomical pacing of late Palaeocene to early Eocene global warming events, *Nature*, *435*, 1083–1087.

Lyle, M. (2003), Neogene carbonate burial in the Pacific Ocean, *Paleoceanography*, *18*(3, 1059), doi:10.1029/2002PA000777.

Lyle, M., and J. Backman (2013), Data report: Calibration of XRF-estimated $CaCO_3$ along the Site U1338 splice, in *Proceedings of the Integrated Ocean Drilling Program*, vol. 320/321, edited by H. Pälike and The Expedition 320/321 Scientists, IODP Manage. Int., Inc., Tokyo, doi:10.2204/iodp.proc.320321.205.2013.

Lyle, M., and J. Baldauf (2015), Biogenic sediment regimes in the Neogene equatorial Pacific, IODP Site U1338: Burial, production, and diatom community, *Palaeogeogr. Palaeoclimatol. Palaeoecol.*, *433*, 106–128, doi:10.1016/j.palaeo.2015.04.001.

Lyle, M., and P. A. Wilson (2006), Leg 199 synthesis: Evolution of the equatorial Pacific in the early Cenozoic, in *Proceedings of the Ocean Drilling Program, Sci. Results*, vol. 199, edited by P. A. Wilson et al., pp. 1–39, Ocean Drilling Program, College Station, Tex.

Lyle, M., J. Barron, T. J. Bralower, M. Huber, A. Olivarez Lyle, A. C. Ravelo, D. K. Rea, and P. A. Wilson (2008), Pacific Ocean and Cenozoic evolution of climate, *Rev. Geophys.*, *46*, RG2002, doi:10.1029/2005RG000190.

Lyle, M., H. Pälike, H. Nishi, I. Raffi, K. Gamage, and A. Klaus (2010), The Pacific equatorial age transect, IODP expeditions 320 and 321: Building a 50-million-year-long environmental record of the equatorial Pacific, *Sci. Drill.*, *9*, 4–15, doi:10.2204/iodp.sd.9.01.2010.

Lynch-Stieglitz, J., T. F. Stocker, W. S. Broecker, and R. G. Fairbanks (1995), The influence of air-sea exchange on the isotopic composition of oceanic carbon: Observations and modeling, *Global Biogeochem. Cycles*, *9*, 653–665, doi:10.1029/95GB02574.

Margolis, S. V., P. M. Kroopnick, D. E. Goodney, W. C. Dudley, and M. E. Mahoney (1975), Oxygen and carbon isotopes from calcareous nannofossils as paleoceanographic indicators, *Science*, *189*, 555–557.
Mayer, L., et al. (1985), Site 573, in *Proceedings of the Deep Sea Drilling Project*, *Init. Rep*., vol. 85, edited by L. Mayer et al., pp. 137–223, Deep Sea Drilling Project, Wash.
Mayer, L., et al. (1992), *Proceedings of the Ocean Drilling Program*, *Init. Rep*., vol. 138, pp. 1–1462, Ocean Drilling Program, College Station, Tex.
McIntyre, A., and R. McIntyre (1971), Coccolith concentrations and differential solution in oceanic sediments, in *The Micropalaeontology of the Oceans*, edited by B. M. Funnell and W. R. Riedel, pp. 253–261, Cambridge Univ. Press, Cambridge, U. K.
Mix, A. C., J. Le, and N. J. Shackleton (1995a), Benthic foraminiferal stable isotope stratigraphy of site 846: 0–1.8 Ma, in *Proceedings of the Ocean Drilling Program*, *Sci. Results*, vol. 138, edited by N. G. Pisias et al., pp. 839–854, College Station, Tex.
Mix, A. C., N. G. Pisias, W. Rugh, J. Wilson, A. Morey, and T. Hagelberg (1995b), Benthic foraminifer stable isotope record from Site 849 (0–5 Ma): Local and global climate changes, in *Proceedings of the Ocean Drilling Program*, *Sci. Results*, vol. 138, edited by N. G. Pisias et al., pp. 371–412, Ocean Drilling Program, College Station, Tex.
Mörth, C. M., and J. Backman (2011), Practical steps for improved estimates of calcium carbonate concentrations in deep sea sediments using coulometry, *Limnol. Oceanogr. Methods*, *9*, 565–570.
Paasche, E. (2001), A review of the coccolithophorid *Emiliania huxleyi* (Prymnesiophyceae), with particular reference to growth, coccolith formation, and calcification—Photosynthesis interactions, *Phycologia*, *40*, 503–529.
Pälike, H., M. W. Lyle, H. Nishi, I. Raffi, K. Gamage, A. Klaus, and the Expedition 320/321 Scientists (2010), Site U1338, in *Proceedings of the Integrated Ocean Drilling Program*, vol. 320/321, edited by H. Pälike et al., 148 pp., IODP Manage. Int., Inc., Tokyo, doi:10.2204/iodp.proc.320321.110.2010.
Pälike, H., et al. (2012), A Cenozoic record of the equatorial Pacific carbonate compensation depth, *Nature*, *488*, 609–615.
Paull, C. K., and H. R. Thierstein (1987), Stable isotopic fractionation among particles in Quaternary coccoliths-sized deep-sea sediments, *Paleoceanography*, *2*, 423–429, doi:10.1029/PA002i004p00423.
Paull, C. K., and H. R. Thierstein (1990), Comparison of fine fraction monospecific foraminiferal stable isotope stratigraphies from pelagic carbonates across the last glacial termination, *Mar. Micropaleontol.*, *16*, 207–217.
Pearson, P. N., and C. E. Burgess (2008), Foraminifer test preservation and diagenesis: Comparison of high latitude Eocene sites, *Geol. Soc. London, Spec. Publ.*, *303*, 59–72.
Pennington, J. T., K. L. Mahoney, V. S. Kuwahara, D. D. Kolber, R. Calienes, and F. P. Chavez (2006), Primary production in the eastern tropical Pacific: A review, *Prog. Oceanogr.*, *69*, 285–317.
Perch-Nielsen, K. (1985), Cenozoic calcareous nannofossils, in *Plankton Stratigraphy*, edited by H. M. Bolli, J. B. Saunders, and K. Perch-Nielsen, pp. 155–262, Cambridge Univ. Press, Cambridge, U. K.
Peterson, L. C., and J. Backman (1990), Late Cenozoic carbonate accumulation and the history of the carbonate compensation depth in the western equatorial Indian Ocean, in *Proceedings of the Ocean Drilling Program*, *Sci. Res*., vol. 115, edited by R. A. Duncan et al., pp. 467–507, Ocean Drilling Program, College Station, Tex.
Pisias, N. G., L. A. Mayer, and A. C. Mix (1995), Paleoceanography of the eastern equatorial Pacific during the Neogene: Synthesis of Leg 138 drilling results, in *Proceedings of the Ocean Drilling Program*, *Sci. Results*, vol. 138, edited by N. G. Pisias et al., pp. 5–21, Ocean Drilling Program, College Station, Tex.
Pujos, A. (1985a), Nannofossils from Quaternary deposits in the high-productivity area of the central equatorial Pacific, Deep Sea Drilling Project Leg 85, in *Proceedings of Deep Sea Drilling Project*, *Init. Rep*., vol. 85, edited by L. Mayer et al., pp. 553–579, Deep Sea Drilling Project, Wash.
Pujos, A. (1985b), Cenozoic nannofossils, central equatorial Pacific, Deep Sea Drilling Project Leg 85, in *Proceedings of Deep Sea Drilling Project*, *Init. Rep*., vol. 85, edited by L. Mayer et al., pp. 581–607, Wash.
Raffi, I., and J.-A. Flores (1995), Pleistocene through Miocene calcareous nannofossils from eastern equatorial Pacific Ocean (Leg 138), in *Proceedings of the Ocean Drilling Program*, *Sci. Results*, vol. 138, edited by N. G. Pisias et al., pp. 233–286, Ocean Drilling Program, College Station, Tex.
Ravelo, A. C. (2010), Palaeoclimate: Warmth and glaciation, *Nat. Geosci.*, *3*, 672–674.
Ravelo, A. C., D. H. Andreasen, M. Lyle, A. Olivarez Lyle, and M. W. Wara (2004), Regional climate shifts caused by gradual global cooling in the Pliocene epoch, *Nature*, *429*, 263–267.
Raymo, M. E., W. F. Ruddiman, J. Backman, B. M. Clement, and D. G. Martinson (1989), Late Pliocene variation in Northern Hemisphere ice sheets and North Atlantic deep water circulation, *Paleoceanography*, *4*, 413–446, doi:10.1029/PA004i004p00413.
Reghellin, D., G. R. Dickens, and J. Backman (2013), The relationship between wet bulk density and carbonate content in sediments from the eastern equatorial Pacific, *Mar. Geol.*, *344*, 41–52.
Révész, K. M., and J. M. Landwehr (2002), ^{13}C and ^{18}O isotopic composition of $CaCO_3$ measured by continuous flow isotope ratio mass spectrometry: Statistical evaluation and verification by application to Devils Hole DH-11 calcite, *Rapid Commun. Mass Spectrom.*, *16*, 2102–2114.
Rickaby, R. E. M., J. Henderiks, and J. N. Young (2010), Perturbing phytoplankton: Response and isotopic fractionation with changing carbonate chemistry in two coccolithophore species, *Clim. Past*, *6*, 771–785.
Romanek, C. S., E. L. Grossman, and J. W. Morse (1992), Carbon isotopic fractionation in synthetic aragonite and calcite: Effects of temperature and precipitation rate, *Geochim. Cosmochim. Acta*, *56*, 419–430.
Schmidt, G. A., G. R. Bigg, and E. J. Rohling (1999), Global seawater oxygen-18 database—V1.21. [Available at http://data.giss.nasa.gov/o18data/.]
Scholle, P. A., and M. A. Arthur (1980), Carbon isotope fluctuation in Cretaceous pelagic limestones: Potential stratigraphic and petroleum exploration tool, *AAPG Bull.*, *64*, 67–87.
Schrag, D. P., D. J. DePaolo, and F. M. Richter (1995), Reconstructing past sea surface temperatures: Correcting for diagenesis of bulk marine carbonate, *Geochim. Cosmochim. Acta*, *59*, 2265–2278.
Schroeder, J. O., R. W. Murray, M. Leinen, R. C. Pflaum, and T. R. Janecek (1997), Barium in equatorial Pacific carbonate sediment: Terrigenous, oxide, and biogenic associations, *Paleoceanography*, *12*, 125–146, doi:10.1029/96PA02736.
Seki, O., D. N. Schmidt, S. Schouten, E. C. Hopmans, J. S. Sinninghe Damsté, and R. D. Pancost (2012), Paleoceanographic changes in the eastern equatorial Pacific over the last 10 Myr, *Paleoceanography*, *27*, PA3224, doi:10.1029/2011PA002158.
Sexton, P. F., P. A. Wilson, and P. N. Pearson (2006), Microstructural and geochemical perspectives on planktic foraminiferal preservation: "Glassy" versus "Frosty", *Geochem. Geophys. Geosystyst.*, *7*, Q12P19, doi:10.1029/2006GC001291.
Shackleton, N. J. (1967), Oxygen isotope analyses and Pleistocene temperatures re-assessed, *Nature*, *215*, 15–17.
Shackleton, N. J. (1986), Paleogene stable isotope events, *Palaeogeogr. Palaeoclimatol. Palaeoecol.*, *57*, 91–102.
Shackleton, N. J., and M. A. Hall (1984), Carbon isotope data from Leg 74 sediments, in *Proceedings of Deep Sea Drilling Program*, *Init. Rep*., vol. 74, edited by T. C. Moore Jr. et al., pp. 613–619, Deep Sea Drilling Project, Wash.

Shackleton, N. J., and M. A. Hall (1995), Stable isotopes records in bulk sediments (Leg 138), in *Proceedings of the Ocean Drilling Program*, *Sci. Results*, vol. 138, edited by N. G. Pisias et al., pp. 797–805, Ocean Drilling Program, College Station, Tex.

Shackleton, N. J., S. Crowhurst, T. Hagelberg, N. G. Pisias, and D. A. Schneider (1995a), A new late Neogene time scale: application to Leg 138 sites, in *Proceedings of the Ocean Drilling Program, Sci. Results*, vol. 138, edited by N. G. Pisias et al., pp. 73–101, Ocean Drilling Program, College Station, Tex.

Shackleton, N. J., M. Hall, and D. Pate (1995b), Pliocene stable isotope stratigraphy of site 846, in *Proceedings of the Ocean Drilling Program*, *Sci. Results*, vol. 138, edited by N. G. Pisias et al., pp. 337–355, Ocean Drilling Program, College Station, Tex.

Slotnick, B. S., G. R. Dickens, M. J. Nicolo, C. J. Hollis, J. S. Crampton, J. C. Zachos, and A. Sluijs (2012), Large-amplitude variations in carbon cycling and terrestrial weathering during the latest Paleocene and earliest Eocene: The record at Mead Stream, New Zealand, *J. Geol.*, *120*, 487–505.

Snoeckx, H., and D. K. Rea (1995), $CaCO_3$ content and bulk density of Leg 138 site-survey piston cores, in *Proceedings of the Ocean Drilling Program*, *Sci. Results*, vol. 138, edited by N. G. Pisias et al., pp. 885–888, Ocean Drilling Program, College Station, Tex.

Spero, H. J. (1998), Life history and stable isotope geochemistry of planktic foraminifera, in *Isotope Paleobiology and Paleoecology*, *Paleontol. Soc. Pap.*, vol. 4, edited by R. D. Norris and R. M. Corfield, pp. 7–36, Paleontol. Soc., Pittsburgh, Pa.

Steinmetz, J. C. (1994), Stable isotopes in modern coccolithophores, in *Coccolithophores*, edited by A. Winter and W. G. Siesser, pp. 219–229 , Cambridge Univ. Press, Cambridge, U. K.

Steinmetz, J. C., and T. F. Anderson (1984), The significance of isotopic and paleontologic results on Quaternary calcareous nannofossil assemblages from Caribbean core P6304-4, *Mar. Micropaleontol.*, *8*, 403–424.

Steph, S., R. Tiedemann, M. Prange, J. Groeneveld, M. Schulz, A. Timmermann, D. Nürnberg, C. Rühlemann, C. Saukel, and G. Haug (2010), Early Pliocene increase in thermohaline overturning pre-conditioned the development of the modern equatorial Pacific cold tongue, *Paleoceanography*, *25*, PA2202, doi:10.1029/2008PA001645.

Stoll, H. M. (2005), Limited range of interspecific vital effects in coccoliths stable isotopic records during the Paleocene-Eocene thermal maximum, *Paleoceanography*, *20*, PA1007, doi:10.1029/2004PA001046.

Tagliabue, A., and L. Bopp (2008), Towards understanding global variability in ocean carbon-13, *Global Biogeochem. Cycles*, *22*, GB1025, doi:10.1029/2007GB003037.

Trenberth, K. E., and J. M. Caron (2000), The Southern Oscillation revisited: Sea level pressures, surface temperatures, and precipitation, *J. Clim.*, *13*, 4358–4365.

Tripati, A., J. Backman, H. Elderfield, and P. Ferretti (2005), Eocene bipolar glaciation associated with global carbon cycle changes, *Nature*, *436*, 341–346.

van Andel, T. J., G. R. Heath, and T. C. Moore Jr. (1975), Cenozoic history and paleoceanography of central equatorial Pacific Ocean: A regional synthesis of Deep-Sea Drilling Project data, *Geol. Soc. Am. Mem.*, *143*, 1–143.

Voigt, S., A. S. Gale, C. Jung, and H. C. Jenkyns (2012), Global correlation of Upper Campanian-Maastrictian successions using carbon-isotope stratigraphy: Development of a new Maastrictian timescale, *Newslett. Stratigr.*, *45*, 25–53.

Wara, M. W., A. C. Ravelo, and M. L. Delaney (2005), Permanent El Nino-like conditions during the Pliocene warm period, *Science*, *309*, 758–761.

Weinreich, N., and F. Theyer (1985), Paleomagnetism of Deep Sea Drilling Project Leg 85 sediments: Neogene magnetostratigraphy and tectonic history of the central equatorial Pacific, in *Proceedings of Deep Sea Drilling Project*, *Init. Rep.*, vol. 85, edited by L. Mayer et al., pp. 849–901, Deep Sea Drilling Project, Wash.

Weissert, H., and E. Erba (2004), Volcanism, CO_2 and palaeoclimate: A Late Jurassic–Early Cretaceous carbon and oxygen isotope record, *J. Geol. Soc.*, *161*, 695–702.

Wilkens, R. H., G. R. Dickens, J. Tian, J. Backman, and the Expedition 320/321 Scientists (2013), Data report: Revised composite depth scales for Sites U1336, U1337, and U1338, in *Proceedings of the Integrated Ocean Drilling Program*, *Proc. IODP*, vol. 320/321, edited by H. Pälike and The Expedition 320/321 Scientists, IODP Manage. Int., Inc., Tokyo, doi:10.2204/iodp.proc.320321.209.2013.

Young, J. R., M. Geisen, and I. Probert (2005), A review of selected aspects of coccolithophore biology with implications for paleobiodiversity estimation, *Micropaleontology*, *51*, 267–288.

Zachos, J. C., M. Pagani, L. Sloan, E. Thomas, and K. Billups (2001), Trends, rhythms, and aberrations in global climate 65 Ma to present, *Science*, *292*, 686–693.

Zachos, J. C., H. McCarren, B. Murphy, U. Röhl, and T. Westerhold (2010), Tempo and scale of late Paleocene and early Eocene carbon isotope cycles: Implications for the origin of hyperthermals, *Earth Planet. Sci. Lett.*, *299*, 242–249.

Zeebe, R. E. (2007), An expression for the overall oxygen isotope fractionation between the sum of dissolved inorganic carbon and water, *Geochem. Geophys. Geosyst.*, *8*, Q09002, doi:10.1029/2007GC001663.

Zeebe, R. E., J. Bijma, and D. A. Wolf-Gladrow (1999), A diffusion–reaction model of carbon isotope fractionation in foraminifera, *Mar. Chem.*, *64*, 199–227.

Zhang, J., P. D. Quay, and D. O. Wilbur (1995), Carbon isotope fractionation during gas-water exchange and dissolution of CO_2, *Geochim. Cosmochim. Acta*, *59*, 107–114.

Zhang, Y. G., M. Pagani, and Z. Liu (2014), A 12-million-year temperature history of the tropical Pacific Ocean, *Science*, *344*, 84–87.

Ziveri, P., H. Stoll, I. Probert, C. Klaas, M. Geisen, G. Ganssen, and J. Young (2003), Stable isotope 'vital effects' in coccolith calcite, *Earth Planet. Sci. Lett.*, *210*, 137–149.

Erratum

In the originally published version of this article, a minor error was discovered in the text. The error has since been corrected and this version may be considered the authoritative version of record.